Bioconjugate Chemistry

Article

pubs.acs.org/bc

# Somatostatin Subtype-2 Receptor-Targeted Metal-Based Anticancer Complexes

Flavia Barragán,[†,‡,#] Dolors Carrion-Salip,[§,#] Irene Gómez-Pinto,[⊥] Alejandro González-Cantó,[†,‡] Peter J. Sadler,[∥] Rafael de Llorens,[§] Virtudes Moreno,[‡] Carlos González,[⊥] Anna Massaguer,*[,§] and Vicente Marchán*[,†]

[†]Departament de Química Orgànica and IBUB and [‡]Departament de Química Inorgànica, Universitat de Barcelona, Martí i Franquès 1-11, E-08028 Barcelona, Spain

[§]Departament de Biologia, Universitat de Girona, Campus Montilivi, E-17071 Girona, Spain

[⊥]Instituto de Química-Física "Rocasolano", CSIC, Serrano 119, E-28006, Madrid, Spain

[∥]Department of Chemistry, University of Warwick, Coventry, CV4 7AL, United Kingdom

Supporting Information

**ABSTRACT:** Conjugates of a dicarba analogue of octreotide, a potent somatostatin agonist whose receptors are overexpressed on tumor cells, with $[PtCl_2(dap)]$ (dap = 1-(carboxylic acid)-1,2-diaminoethane) (**3**), $[(\eta^6\text{-bip})Os(4\text{-}CO_2\text{-pico})Cl]$ (bip = biphenyl, pico = picolinate) (**4**), $[(\eta^6\text{-}p\text{-cym})RuCl(dap)]^+$ (*p*-cym = *p*-cymene) (**5**), and $[(\eta^6\text{-}p\text{-cym})RuCl(imidazole\text{-}CO_2H)(PPh_3)]^+$ (**6**), were synthesized by using a solid-phase approach. Conjugates **3**–**5** readily underwent hydrolysis and DNA binding, whereas conjugate **6** was inert to ligand substitution. NMR spectroscopy and molecular dynamics calculations showed that conjugate formation does not perturb the overall peptide structure. Only **6** exhibited antiproliferative activity in human tumor cells ($IC_{50}$ = 63 ± 2 $\mu$M in MCF-7 cells and $IC_{50}$ = 26 ± 3 $\mu$M in DU-145 cells) with active participation of somatostatin receptors in cellular uptake. Similar cytotoxic activity was found in a normal cell line ($IC_{50}$ = 45 ± 2.6 $\mu$M in CHO cells), which can be attributed to a similar level of expression of somatostatin subtype-2 receptor. These studies provide new insights into the effect of receptor-binding peptide conjugation on the activity of metal-based anticancer drugs, and demonstrate the potential of such hybrid compounds to target tumor cells specifically.

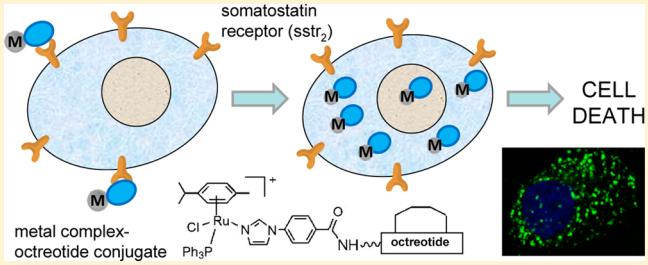


## INTRODUCTION

The overexpression of the receptors for many regulatory peptides in human tumor cells in comparison to their expression in normal cells has prompted research on the use of such peptides in tumor targeting for both diagnostic and therapeutic purposes.[1−3] From the therapeutic point of view, a promising approach for the treatment of cancer consists of the attachment of a cytotoxic drug to a peptide moiety with the aim of improving its activity and bioavailability. This targeted anticancer strategy will result in therapeutic agents with increased tumor selectivity and decreased toxicity in normal tissues.

Among natural receptor-binding peptides, the neuroendocrine hormone somatostatin and its analogues have received much attention because of their high affinity against its five human receptors ($sst_1$−$sst_5$).[1,3,4] These receptors are overexpressed in various major tumor types, including lung, breast, prostate, adrenal, and neuroendocrine tumors in comparison with normal tissues.[5] The successful use of radiolabeled somatostatin for imaging and radionuclide therapy has prompted the development of new cyclic and acyclic analogues with better receptor affinity and higher stability under physiological conditions.[6]

Octreotide,[7] **1** (Chart 1), a metabolically stabilized cyclooctapeptide analogue of somatostatin that includes D-amino acids to enhance resistance to enzymatic degradation and a cystine bridge to stabilize the pharmacophore $\beta$-turn, is particularly interesting because of its high affinity and selectivity for the receptor $sst_2$,[6] which is the receptor subtype most frequently found on tumor cells. This selectivity has allowed the development of derivatives such as [$^{111}$In-DTPA]-octreotide and [$^{90}$Y-DOTA-Tyr$^3$]-octreotide which are used in the clinics for molecular imaging and therapy of neuroendocrine tumors, respectively.[8] Octreotide has also been conjugated to cytotoxic organic compounds such as doxorubicin, camptothecin, and paclitaxel, with promising results in some cases because of the reduced toxicity and the increased selectivity of the conjugates compared with that of the free drug.[4,9]

**Received:** March 30, 2012
**Revised:** August 6, 2012
**Published:** August 8, 2012

**Chart 1. Structure of the Conjugates Synthesized**[a]

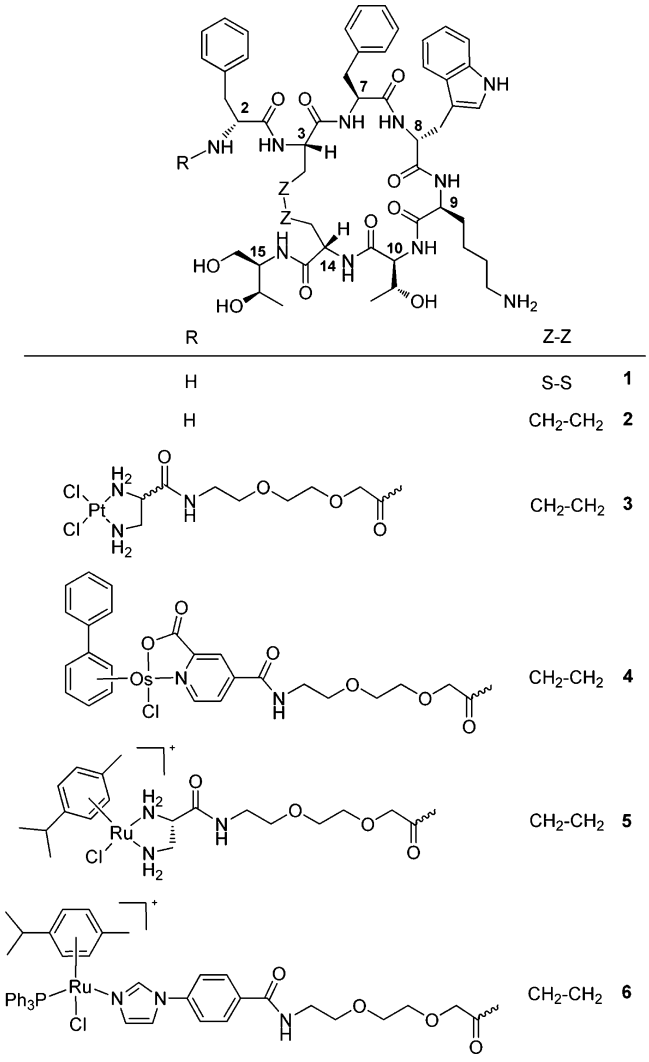


[a]Numbering of the amino acid residues follows that of native somatostatin.

Despite the successful history of cisplatin and its second-generation derivatives (carboplatin and oxaliplatin) in the treatment of some types of cancer,[10] the severe toxic side-effects and the acquired or intrinsic resistance of certain tumors has focused research on other metal-based complexes in an effort to develop improved chemotherapeutic agents.[11,12] Indeed, in addition to several platinum compounds, two ruthenium(III) coordination complexes, *trans*-[$RuCl_4$(DMSO)-(Im)]ImH (NAMI-A) and *trans*-[$RuCl_4(Ind)_2$]IndH (NKP-1339), are currently on clinical trials.[13,14]

In recent years, research on bioinorganic chemistry has also been focused on organometallic ruthenium(II) and osmium(II) arene complexes, since these compounds have shown promising *in vitro* and *in vivo* anticancer activities, including cell lines that have become resistant to cisplatin.[15−19] Ruthenium and its heavier congener osmium offer several advantages in comparison with platinum compounds, including the ability to bind to a wide variety of types of ligands, the availability of additional coordination sites in octahedral complexes, the possibility of controlling the shape of the complex, and the changes in the oxidation state. It is also particularly relevant that they have the capacity to undergo ligand exchange in a similar way to cisplatin, which makes them particularly attractive for developing new anticancer drugs. Unlike cisplatin, which has two reactive Pt−Cl coordination bonds, some active organometallic piano-stool complexes have only one reactive site (Ru/Os−Cl). The aquation of the chlorido complexes, mostly suppressed in extracellular fluids (chloride concentration ∼100 mM), is triggered inside the cell nucleus by the low chloride concentration (4 mM), allowing the interaction of the active aqua species with biomolecules such as DNA.[20−22]

On the basis of these precedents, a promising approach in the search of new metal-based anticancer drugs would consist of the conjugation of platinum and classical nonplatinum metal complexes (e.g., ruthenium and osmium) to carrier molecules such as receptor-binding peptides. Indeed, given the over-expression of selective receptors for these peptides on the membrane of tumoral cells, it is expected that the peptide sequences will have a positive effect on the therapeutic properties of the metal-based drug (e.g., reduction of the toxic side-effects) since they will act as a "tumour-targeting devices". With this idea in mind, we have synthesized conjugates between a dichloridoplatinum(II) complex and octreotide derivatives in which the disulfide bond had been replaced by $CH_2$—$CH_2$ or CH═CH linkages.[23] This chemical modification on the peptide does not substantially alter the binding affinity of the dicarba-octreotide analogues for the $sst_2$ receptor but increases the stability of the carrier biomolecule in the reductive cellular environment.[24] In addition, we have recently described the synthesis and DNA ruthenation under visible light irradiation of a photoactivated ruthenium(II) arene complex conjugated to a dicarba analogue of octreotide.[25] In recent years, several coordination or organometallic complexes have also been conjugated to carrier molecules such as receptor-binding peptides or known delivery peptides to improve both cellular uptake to cancer cells and cytotoxic activity of the metal-based drug.[26−33]

Herein, we report on the use of conjugates between octreotide and several metal complexes as new chemotherapeutic agents. In particular, the synthesis of hybrid compounds between the dicarba analogue of octreotide (**2**) and platinum(II), ruthenium(II), and osmium(II) metal complexes has been accomplished by efficient solid-phase procedures (compounds **3**−**6** in Chart 1). The influence of the attachment of the metal complex on the structure of octreotide has been studied by NMR spectroscopy and molecular dynamics, as well as the capacity of these conjugates to bind DNA. Finally, cellular uptake and cytotoxicity studies have been carried out in a normal cell line and two human tumoral cell lines.

## EXPERIMENTAL PROCEDURES

**Materials and Methods.** Unless otherwise stated, common chemicals and solvents (HPLC-grade or reagent-grade quality) were purchased from commercial sources and used without further purification. Peptide-grade DMF was from Scharlau. Fmoc-protected amino acids, resins, and coupling reagents for solid-phase synthesis were obtained from Novabiochem, Bachem, or Iris Biotech. Fmoc-Hag-OH was purchased from Bachem. Fmoc-L-threoninol *p*-carboxyacetal was synthesized following previously reported procedures.[34] Solid-phase syntheses were performed manually in a polypropylene syringe fitted with a polyethylene disk. Second-generation Grubbs catalyst and Wilkinson's catalyst were purchased from Aldrich.


dx.doi.org/10.1021/bc300173h | *Bioconjugate Chem.* 2012, 23, 1838−1855

Milli-Q water was directly obtained from a Milli-Q system equipped with a 5000 Da ultrafiltration cartridge. Metal complexes (±)-[$PtCl_2$(dap)] (**7**),[23] (±)-[$PtCl_2$(Etdap)] (**15**),[35] [($\eta^6$-bip)Os(4-$CO_2$-pico)Cl] (**8**),[36] [{($\eta^6$-*p*-cym)Ru($\mu$-Cl)Cl}$_2$] (**9**), [($\eta^6$-*p*-cym)$RuCl_2(PPh_3)$] (**10**),[37] and [($\eta^6$-*p*-cym)$RuCl(PPh_3)_2][PF_6$] (**11**)[38] were synthesized and characterized as previously described. L-2,3-Diaminopropionic acid methyl ester dihydrochloride[39] and $N^{\alpha}$,$N^{\beta}$-bis-(9-fluorenylmethyloxycarbonyl)-L-2,3-diaminopropionic acid[40] were synthesized as previously described. 5(6)-Carboxyfluorescein was purchased from Aldrich and octreotide acetate from Bachem. All the assayed compounds displayed a purity of ≥95%, determined by HPLC analysis.

The human breast cancer cell line MCF-7 and the human prostate carcinoma cell line DU-145 were obtained from the American Tissue Culture Collection (ATTC, Rockville, MD, USA). Chinese hamster ovary (CHO) cells were used as a nontumor cell line. The cells were maintained in Dulbecco's modified Eagle's medium supplemented with 10% fetal bovine serum and 1% penicillin−streptomycin (GIBCO BRL, Grand Island, NY) at 37 °C in a humidified atmosphere containing 5% $CO_2$. The cells were passaged two times per week.

NMR spectra were recorded at 25 °C on Varian Gemini 300 MHz and Varian Mercury 400 MHz spectrometers using deuterated solvents. Tetramethylsilane (TMS) was used as an internal reference ($\delta$ 0 ppm) for $^1$H spectra recorded in $CDCl_3$ and the residual signal of the solvent ($\delta$ 77.16 ppm) for $^{13}$C spectra. For $CD_3OD$, acetone-$d_6$, DMSO-$d_6$, or $D_2O$, the residual signal of the solvent was used as a reference.

High-resolution MALDI-TOF mass spectra were recorded on a 4800 Plus MALDI-TOF/TOF spectrometer (Applied Biosystems) in the positive-ion mode using 2,4-dihidroxybenzoic acid as a matrix. ESI mass spectra (ESI-MS) were recorded on a Micromass ZQ instrument with single quadrupole detector coupled to an HPLC. High-resolution electrospray mass spectra (HR ESI MS) were obtained on an Agilent 1100 LC/MS-TOF instrument.

**Synthesis of Metal−Octreotide Conjugates (3−6 and 12) and Fluorescein-Labeled Peptides (13−14).** Solid-phase peptide synthesis was performed on a Rink amide resin-*p*-MBHA ($f$ = 0.34 mmol/g, 100−200 mesh) using standard Fmoc/tBu chemistry with the following side-chain protecting groups: Boc ($N^i$-*tert*-butoxicarbonyl, tryptophan, and $N^e$-*tert*-butoxicarbonyl, lysine), $^t$Bu (*O*-*tert*-butyl, threonine), and Trt (*S*-trityl, cysteine). The assembly of the dicarba analogue of octreotide was performed as previously described.[23,24] Briefly, Fmoc-L-threoninol *p*-carboxyacetal (1.8 mol equiv) was first coupled using DIPC (1.8 mol equiv) and HOBt (1.8 mol equiv) in anhydrous DMF for 1 h. The following Fmoc-protected amino acids (2.4 mol equiv) were incorporated with HATU (2.3 mol equiv) and DIPEA (4.8 mol equiv) in anhydrous DMF for 1 h. Microwave-assisted ring-closing methatesis using second-generation Grubbs catalyst and hydrogenation reaction with Wilkinson's catalyst were carried out as previously described.[23] Finally, 8-(9-fluorenylmethyloxycarbonyl-amino)-3,6-dioxaoctanoic acid (3 mol equiv) or $\gamma$-aminoisobutyric acid (3 mol equiv) were coupled onto the cyclic dicarba analogue of octreotide **2** bound to resin with DIPC (3 mol equiv) and HOAt (3 mol equiv) in anhydrous DMF for 1 h. After removal of the Fmoc group (20% piperidine in DMF) from the Fmoc-protected linker-derivatized dicarba analogue of octreotide bound to resin, coupling or assembly of the metal complexes on the free *N*-terminal end was carried out as indicated for each metal. The reactor was protected from light by covering it with aluminum foil.

Side-chain deprotection and cleavage from the resin was performed simultaneously with TFA/TIS/$H_2O$ 95:2.5:2.5 (peptides, fluorescein-labeled dicarba octreotide **13** and conjugate **4**), TFA/phenol/$H_2O$ 95:2.5:2.5 (conjugates **3**, **5**, **6**, and **12**), or TFA/$H_2O$/TIS/EDT 94:2.5:2.5:1 (fluorescein-labeled octreotide **14**) for 1 h at room temperature. Most of the TFA was removed by bubbling $N_2$ into the solution, and the resulting residue was poured onto cold ether to precipitate the target compound.

Analytical reversed-phase HPLC analyses were carried out on a GraceSmart RP $C_{18}$ column (250 × 4 mm, 5 $\mu$m, flow rate: 1 mL/min), using linear gradients of 0.045% TFA in $H_2O$ (solvent A) and 0.036% TFA in ACN (solvent B). In some cases, small-scale purification was carried out using the same column. Large-scale purification was carried out on a Jupiter Proteo semipreparative column (250 × 10 mm, 10 $\mu$m, flow rate: 3−4 mL/min), using linear gradients of 0.1% TFA in $H_2O$ (solvent A) and 0.1% TFA in ACN (solvent B). After several runs, pure fractions were combined and lyophilized.

*Platinum−Octreotide Conjugate* ***3***. [$PtCl_2$(dap)] (5 mol equiv) was coupled with DIPC (5 mol equiv) and NHS (10 mol equiv) in anhydrous DMF for 15 h at rt. Overall yield (synthesis + purification): 14%. Characterization: $R_t$ = 14.2 min (analytical gradient: 20% to 60% in 30 min); HR ESI MS, positive mode: $m/z$ 1479.5574 (calcd mass for $C_{60}H_{88}Cl_2N_{13}O_{14}Pt$ $[M+H]^+$: 1479.5598); HR MALDI-TOF MS, positive mode: $m/z$ 1479.85 (calcd mass for $C_{60}H_{88}Cl_2N_{13}O_{14}Pt$ $[M+H]^+$: 1479.5598), $m/z$ 1501.87 (calcd mass for $C_{60}H_{87}Cl_2N_{13}NaO_{14}Pt$ $[M+Na]^+$: 1501.5418).

*Osmium−Octreotide Conjugate* ***4***. [($\eta^6$-bip)Os(4-$CO_2$-pico)Cl] (5 mol equiv) was coupled with DIPC (5 mol equiv) and HOAt (5 mol equiv) in anhydrous DMF for 3 h at rt. Overall yield (synthesis + purification): 16%. Characterization: $R_t$ = 20.2 min (analytical gradient: 20% to 60% in 30 min); HR ESI MS, positive mode: $m/z$ 1657.6621 (calcd mass for $C_{76}H_{94}ClN_{12}O_{16}Os$ $[M+H]^+$: 1657.6214); HR MALDI-TOF MS, positive mode: $m/z$ 1679.60 (calcd mass for $C_{76}H_{92}ClN_{12}NaO_{16}Os$ $[M+Na]^+$: 1679.6034).

*Ruthenium(dap)−Octreotide Conjugate* ***5***. $N^{\alpha}$,$N^{\beta}$-Bis-(9-fluorenylmethyloxycarbonyl)-L-2,3-diaminopropionic acid (4 mol equiv) was coupled with HATU (3.9 mol equiv) in anhydrous DMF in the presence of DIPEA (8 mol equiv) for 1 h at rt. After removal of the Fmoc protecting groups, octreotide-bound resin was reacted with **9** (3 mol equiv) in the presence of LiCl (6.6 mol equiv) and $NEt_3$ (7.2 mol equiv) in a DMF/EtOH 9:1 mixture at 100 °C for 1 h under microwave irradiation (40 W). Overall yield (synthesis + purification): 10%. Characterization: $R_t$ = 14.1 min (analytical gradient: 20% to 60% in 30 min); HR MALDI-TOF MS, positive mode: $m/z$ 1448.40 (calcd mass for $C_{70}H_{100}N_{13}O_{14}Ru$ $[M-Cl-H]^+$: 1448.6556).

*Ruthenium−Octreotide Conjugate* ***6***. 4-(1*H*-Imidazol-1-yl)benzoic acid (10 mol equiv) was first coupled with DIPC (10 mol equiv) and HOBt (10 mol equiv) in anhydrous DMF for 1 h at rt. Then, imidazole-derivatized peptide-bound resin was reacted with **11** (3 mol equiv) in the presence of LiCl (3.3 mol equiv) and $NEt_3$ (20 mol equiv) in a DMF/EtOH 9:1 mixture for 8 h at 50 °C. Overall yield (synthesis + purification): 12%. Characterization: $R_t$ = 14.6 min (analytical gradient: 30% to 100% in 30 min); HR ESI MS, positive mode: $m/z$ 1830.7240 (calcd mass for $C_{95}H_{116}ClN_{13}O_{14}PRu$ $[M]^+$:

1830.7234), *m/z* 915.8672 (calcd mass for $C_{70}H_{102}ClN_{13}O_{14}Ru$ $[M+H]^{2+}$: 915.8656); HR MALDI-TOF MS, positive mode: *m/z* 1795.44 (calcd mass for $C_{95}H_{115}N_{13}O_{14}PRu$ $[M-Cl-H]^{+}$: 1794.7468).

*Ruthenium–Octreotide Conjugate* ***12***. Characterization: $R_t$ = 17.7 min (analytical gradient: 30% to 100% in 30 min); HR ESI MS, positive mode: *m/z* 1768.6863 (calcd mass for $C_{93}H_{112}ClN_{13}O_{12}PRu$ $[M]^{+}$: 1768.6867), *m/z* 884.8481 (calcd mass for $C_{70}H_{102}ClN_{13}O_{14}Ru$ $[M+H]^{2+}$: 884.8478). The MS data correspond to the dicarba analogue of octreotide with CH=CH linkage.

*Fluorescein-Labeled Dicarba Analogue of Octreotide* ***13***. Resin-bound linker-derivatized dicarba analogue of octreotide was allowed to react with 5(6)-carboxyfluorescein (5 mol equiv), DIPC (5 mol equiv), and HOAt (5 mol equiv) in anhydrous DMF for 16 h, protected from light. After filtration and washing, peptide-bound resin was treated with 20% piperidine/DMF (2 × 45 min). Overall yield (synthesis + purification): 40%. Characterization: $R_t$ = 23.3 min (analytical gradient: 20% to 60% in 30 min); HR ESI MS, positive mode: *m/z* 1486.6572 (calcd mass for $C_{78}H_{92}N_{11}O_{19}$ $[M+H]^{+}$: 1486.6571).

*Fluorescein-Labeled Octreotide* ***14***. Linear fluorescein-linker-derivatized octreotide was assembled on a Rink amide resin as described above with minor modifications: Fmoc-Hag-OH was replaced by Fmoc-Cys(Trt)-OH and all Fmoc-protected amino acids, Fmoc-linker-OH and 5(6)-carboxy-fluorescein (5 mol equiv) were coupled with DIPC (5 mol equiv) and HOAt (5 mol equiv) in anhydrous DMF. After treatment with 20% piperidine/DMF (2 × 45 min) and acidic cleavage and deprotection, the linear peptide was dissolved (final concentration *ca.* 1 mM) in an aqueous ammonium hydrogen carbonate solution (5%, pH 7.7) and stirred at room temperature for 72 h (some drops of DMSO and MeOH were added after 24 h to improve solubility as well as to increase the oxidation rate). Overall yield (synthesis + purification): 15%. Characterization: $R_t$ = 23.5 min (analytical gradient: 20% to 60% in 30 min); HR-ESI MS, positive mode: *m/z* 1522.5673 (calcd mass for $C_{76}H_{88}N_{11}O_{19}S_2$ $[M+H]^{+}$: 1522.5699).

**Synthesis of Metal Complexes.** *[($\eta^6$-p-cym)RuCl(dap)]-[$PF_6$]* ***(16)***. L-2,3-Diaminopropionic acid methyl ester dihydrochloride (0.068 g; 0.359 mmol) was reacted with complex **9** (0.1 g; 0.163 mmol) and $NEt_3$ (513 μL; 1.63 mmol) in MeOH (15 mL). The mixture was stirred at room temperature for 3 h. The resulting solution was filtered and the volume of the filtrate reduced (to *ca.* 7 mL) in a rotary evaporator. Solid $NH_4PF_6$ (10 mol equiv) was added to the solution and stirred at room temperature for 4 h. The resulting orange microcrystalline solid was filtered, washed with cold MeOH (10 mL), and dried *in vacuo* (68 mg, 40%). $^1$H NMR (400 MHz, DMSO-$d_6$) δ (ppm): 1.22 (6H, d, *J* = 6.8 Hz), 2.15 (3H, s), 2.16–2.31 (2H, m); 2.7 (1H, sp, *J* = 6.8 Hz), 3.02 (1H, br s); 5.04–5.14 (2H, br m), 5.32 (1H, d, *J* = 5.6 Hz), 5.46 (1H, d, *J* = 6 Hz), 5.63 (1H, d, *J* = 6 Hz), 6.67 (1H, d, *J* = 5.6 Hz), 5.88–5.97 (2H, br m). $^{13}C\{^1H\}$ NMR (100 MHz, DMSO-$d_6$) δ (ppm): 18.0, 22.5, 30.4, 58.9, 78.6, 79.4, 80.8, 81.2, 95.7, 101.6, 176.8. HR ESI MS, positive mode: *m/z* 339.0650 (calcd mass for $C_{13}H_{21}N_2O_2Ru$ $[M-Cl-H]^{+}$: 339.0646). HR ESI MS, negative mode: *m/z* 373.0228 (calcd mass for $C_{13}H_{20}ClN_2O_2Ru$ $[M-2H]^{-}$: 373.0255).

*[($\eta^6$-p-cym)RuCl$_2$(Im-BzCOOMe)]*. A suspension of **9** (200 mg, 0.33 mmol) in 10 mL of DCM was reacted with the methyl ester of the 4-(1*H*-Imidazol-1-yl)benzoic acid (1 mol equiv) and stirred at room temperature. Slowly, the suspension dissolved, and after 4 h, diethyl ether was added with stirring to the resulting orange solution until it became turbid. The separated red microcrystalline product was isolated by filtration, washed several times with ether, and dried under vacuo (165 mg, 50%). $^1$H NMR (400 MHz, $CDCl_3$) δ (ppm): 1.31 (6H, d, *J* = 6.8 Hz), 2.24 (3H, s), 3.03 (1H, sp, *J* = 6.8 Hz), 3.95 (3H, s), 5.32 (2H. d, *J* = 5.4 Hz), 5.51 (2H. d, *J* = 5.4 Hz), 7.32 (1H, s), 7.43 (2H, d, *J* = 8.4 Hz), 7.53 (1H, s), 8.14 (2H, d, *J* = 8.4 Hz), 8.38 (s, 1H). $^{13}C\{^1H\}$ NMR (100 MHz, $CDCl_3$) δ (ppm): 20.1, 23.8, 32.2, 54.0, 83.0, 84.0, 100.0, 104.4, 119.9, 122.4, 131.6, 133.1, 135.0, 139.9, 140.9, 167.2.

*[($\eta^6$-p-cym)RuCl(Im-BzCOOMe)($PPh_3$)][$PF_6$]* ***(17)***. Complex [($\eta^6$-*p*-cym)$RuCl_2$(Im-BzCOOMe)] (81 mg, 0.16 mmol) was reacted with $PPh_3$ (1 mol equiv) in methanol (5 mL) for 1 h under reflux. The resulting yellow solution was cooled to room temperature and ammonium hexafluorophosphate (1.1 mol equiv) dissolved in methanol (1 mL) was added. A yellow crystalline solid was filtered off and washed several times with methanol and diethyl ether (106 mg, 90%). $^1$H NMR (400 MHz, acetone-$d_6$) δ (ppm): 1.19 (6H, dd, *J* = 7.2 Hz), 1.83 (3H, s), 2.60 (1H, sp, *J* = 7.2 Hz), 3.93 (3H, s), 5.36 (1H, dt, *J* = 6 Hz), 5.87 (1H, d, *J* = 6 Hz), 6.07 (1H, d, *J* = 6 Hz), 6.20 (1H, d, *J* = 6 Hz), 7.44–7.54 (17H, m), 7.65 (2H, dt, *J* = 10.4 Hz), 8.15 (2H, d, *J* = 8.8 Hz), 8.41 (1H, s). $^{31}P\{^1H\}$ NMR (acetone-$d_6$) δ (ppm): 36.51 (s). $^{13}C\{^1H\}$ NMR (100 MHz, acetone-$d_6$) δ (ppm): 19.1, 22.3, 24.2, 32.7, 53.9, 87.9, 90.2, 90.8, 95.7, 95.8, 105.0, 115.2, 115.3, 121.8, 123.1, 130.2, 130.3, 132.0, 132.1, 132.5, 132.9, 132.8, 133.0, 136.1, 136.2, 141.1, 141.3, 167.1. HR-ESI MS, positive mode: *m/z* 735.1488 (calcd mass for $C_{39}H_{39}ClN_2O_2PRu$ $[M]^{+}$: 735,1481), *m/z* 533.0729 (calcd mass for $C_{28}H_{29}ClPRu$ $[M-(Im-BzCOOMe)]^{+}$: 533.0739), *m/z* 497.0959 (calcd mass for $C_{28}H_{28}PRu$ $[M-(Im-BzCOOMe)-Cl-H]^{+}$: 497.0972).

**DNA Binding Studies.** Complexation reactions were carried out in $H_2O$ (4 mM NaCl) at 37 °C. The required volume of an aqueous solution of the corresponding metal–octreotide conjugate was mixed with the required volume of an aqueous solution of 5′dCATGGCT (1–2 mol equiv). Regarding conjugate **5**, DNA binding studies were performed with the analogue with the CH=CH linkage isoster of octreotide (denoted as **5a**). In all cases, the solutions were 100 μM in the oligonucleotide. The evolution of the reactions was monitored by reversed-phase HPLC on Kromasil $C_{18}$ columns (250 × 4.6 mm, 10 μm, flow rate: 1 mL/min), using linear gradients of aqueous triethylammonium acetate (0.05 M) (solvent A) and ACN (solvent B) or ACN/$H_2O$ 1:1 (solvent B′). Metal adducts were isolated after several HPLC runs by using analytical separation conditions. HR MALDI-TOF MS analysis was carried out in the negative mode using 2,4,6-trihidroxyacetophenone matrix with ammonium citrate as an additive. Enzymatic digestions with 5′- and 3′-exonucleases (bovine spleen and snake venom phosphodiesterases, respectively) were performed as previously described.[41−43]

*Adduct 5′dCATGGCT-conjugate* ***3***. $R_t$ = 11.0 min (gradient: 15% to 50% B in 30 min); HR MALDI-TOF MS, negative mode: *m/z* 3501.0 (calcd mass for $C_{128}H_{171}N_{38}O_{55}P_6Pt$ $[M-3H]^{-}$: 3500.95). MALDI-TOF MS after digestion with snake venom phosphodiesterase: *m/z* 2907.9 (-pCpT) (calcd mass for $C_{109}H_{146}N_{33}O_{42}P_4Pt$ $[M-3H]^{-}$: 2907.89). MALDI-TOF MS after digestion with bovine spleen phosphodiesterase: *m/z* 2594.8 (-CpApTp) (calcd mass for $C_{99}H_{134}N_{28}O_{37}P_3Pt$ [M-


dx.doi.org/10.1021/bc300173h | *Bioconjugate Chem.* 2012, 23, 1838–1855

3H]$^-$: 2594.83), *m/z* 2898.9 (-CpAp) (calcd mass for $C_{109}H_{147}N_{30}O_{44}P_4Pt$ [M-3H]$^-$: 2898.88).

*Adduct 5′dCATGGCT-conjugate* ***4***. $R_t$ = 21.2 min (gradient: 5% to 90% B′ in 30 min); HR MALDI-TOF MS, negative mode: *m/z* 3715.8 (calcd mass for $C_{144}H_{178}N_{37}O_{57}OsP_6$ [M-2H]$^-$: 3715.02). MALDI-TOF MS after digestion with snake venom phosphodiesterase: *m/z* 2793.0 (-pGpCpT) (calcd mass for $C_{115}H_{141}N_{27}O_{38}OsP_3$ [M-2H]$^-$: 2792.88). MALDI-TOF MS after digestion with bovine spleen phosphodiesterase: *m/z* 2808.9 (-CpApTp) (calcd mass for $C_{115}H_{141}N_{27}O_{39}OsP_3$ [M-2H]$^-$: 2808.87), *m/z* 3113.9 (-CpAp) (calcd mass for $C_{125}H_{154}N_{29}O_{46}OsP_4$ [M-2H]$^-$: 3112.92).

*Adduct 5′dCATGGCT-conjugate* ***5a***. $R_t$ = 20.5 min (gradient: 5% to 90% B′ in 30 min); HR MALDI-TOF MS, negative mode: *m/z* 3540.8 (calcd mass for $C_{138}H_{183}N_{38}O_{55}P_6Ru$ [M-3H]$^-$: 3540.02). MALDI-TOF MS after digestion with snake venom phosphodiesterase: *m/z* 2617.6 (-pGpCpT) (calcd mass for $C_{109}H_{146}N_{28}O_{36}P_3Ru$ [M-3H]$^-$: 2617.87). MALDI-TOF MS after digestion with bovine spleen phosphodiesterase: *m/z* 2633.7 (-CpApTp) (calcd mass for $C_{109}H_{146}N_{28}O_{37}P_3Ru$ [M-3H]$^-$: 2633.87), *m/z* 2937.7 (-CpAp) (calcd mass for $C_{119}H_{159}N_{30}O_{44}P_4Ru$ [M-3H]$^-$: 2937.91).

**NMR Spectroscopy.** The samples of the conjugates were prepared by dissolving the appropriate amount of compound in 500 μL of $H_2O$/DMSO-$d_6$ 8:2 to give 0.8 mM solutions. NMR spectra were acquired on Bruker Avance spectrometers operating at 600 or 800 MHz, and processed with *Topspin* software. NOESY experiments were acquired with mixing times of 150 and 300 ms, and TOCSY spectra were recorded with standard MLEV-17 spin-lock sequence, and 80 ms mixing time. Water suppression in $H_2O$ experiments was achieved by including a WATERGATE module in the pulse sequence prior to acquisition. NMR experiments were carried out at temperatures ranging from 0 to 25 °C. The spectral analysis program *Sparky*[44] was used for semiautomatic assignment of the NOESY cross-peaks and quantitative evaluation of the NOE intensities. Sequential assignment of the peptide moiety was carried out using standard $^1$H NMR techniques.

**Structural Modeling.** Molecular dynamics calculations were carried out with the program *Sybyl X-1.3* (Tripos Inc.). Ten initial models for each conjugate were built from the dicarba analogue of octreotide **2** coordinates.[24] Metal complex coordinates were built from crystallographic structures of similar compounds.,[36,45] Each of the initial structures was minimized and then submitted to 300 ps of molecular dynamics simulations. Explicit solvent and periodic boundary conditions were included in the calculations. The last 50 ps of each run was averaged and energy-minimized. Backbone geometry of those peptide residues that do not exhibit significant chemical shift variations was loosely constrained by imposing dihedral angle restraints. Analysis of the representative structures was carried out with the programs *Sybyl* and *MOLMOL*.[46]

**Immunocytochemistry.** MCF-7 cells were seeded on fibronectin-coated coverslips and allowed to attach overnight. Then, the cells were incubated at 37 °C with medium containing 50 μM of **13** during 1, 3, and 6 h, or with medium alone as control. After that, the cells were washed with cold PBS (Gibco BRL) and fixed with 4% paraformaldehyde in PBS for 15 min at 4 °C. The cells nucleus were stained with 2 μg/mL Hoescht 33258 (excitation/emission: 352 nm/461 nm) during 15 min. After washing twice with cold PBS, the cells coverslips were mounted using a fluorescence mounting medium (Dako, Carpinteria, CA, USA) and examined using a Leica TCS-SP5 multiphoton and high-velocity spectral confocal microscope (Leica Microsystems, Nussloch, Germany).

**Internalization Experiments with 13 and 14.** The uptake efficiency of **13** and **14** by the cells was quantified by flow cytometry. The cells were seeded onto 12-well plates and allowed to attach for 24 h. Next, the cells were treated at 37 °C with 50 μM of either **13** or **14** during 1, 3, and 6 h. After rinsing the cells three times with cold PBS, the cells were harvested by trypsinization and the fluorescence of the cells, corresponding to the uptake of the fluorescein-modified peptides, was analyzed using a FACSCalibur (Becton Dickinson Immunocytometry Systems, San Jose, CA) equipped with the *CellQuest* software (Becton Dickinson). Fluorescence intensity was represented on a 4 orders of magnitude log scale (1−10 000). Ten thousand cells were analyzed in each experiment.

**Cytotoxicity Assays.** The cytotoxicity of the conjugates and of the control complexes in MCF-7, DU-145, and CHO cells was determined by the MTT assay. Aliquots of 4000 DU-145 cells, 3500 MCF-7, or 2000 CHO cells were seeded onto flat-bottomed 96-well plates. Twenty-four hours later, the cells were treated for 72 h with the compounds at concentrations ranging from 0 μM to 250 μM. After removal of the treatment, the cells were washed with PBS and incubated for 3 additional hours with 100 μL of fresh culture medium together with 10 μL of MTT (Sigma-Aldrich). The medium was discarded and DMSO (Sigma-Aldrich) was added to each well to dissolve the purple formazan crystalls. Plates were agitated at room temperature for 10 min, and the absorbance of each well was determined on a Multiscan Plate Reader (ELX800, Biotek, Winooski, USA) at a wavelength of 570 nm. Three replicates were used in each experiment. For each treatment, the cell viability was determined as a percentage of the control untreated cells, by dividing the mean absorbance of each treatment by the mean absorbance of the untreated cells. The concentration that reduces by 50% the cell viability ($IC_{50}$) was established for each compound.

**Ruthenium Accumulation in Cancer Cells.** For ruthenium cellular uptake studies, 1.5 × $10^6$ MCF-7 cells were plated in 100 mm Petri dishes and allowed to attach for 48 h. Next, the plates were exposed to the ruthenium−octreotide conjugate **6** or to the unconjugated ruthenium complex **17** at a concentration corresponding to a fifth of their $IC_{50}$ (12.5 μM and 0.66 μM, respectively). Additional plates were incubated with medium alone as negative control. After 24 h of incubation, the cells were rinsed three times with cold PBS and harvested by trypsinization. The number of cells in each sample was counted manually in a hemocytometer using the Trypan blue dye exclusion test. Then, the cells were centrifuged to obtain the whole cell pellet for ICP-MS analysis. All experiments were conducted in triplicate.

**ICP-MS Analysis.** The whole cell pellets were dissolved in 300 μL of concentrated 72% v/v nitric acid, and the samples were then transferred into Wheaton v-vials (Sigma-Aldrich) and heated in an oven at 373 K for 18 h. The vials were then allowed to cool, and each cellular sample solution was transferred into a volumetric tube and combined with washings with Milli-Q water (1.7 mL). Digested samples were diluted 10 times with Milli-Q to obtain a final $HNO_3$ concentration of approximately 2.5% v/v. Ruthenium content was analyzed on an ICP-MS Perkin-Elmer Elan 6000 series machine at the Centres Científics I Tecnològics of the Universitat de Barcelona. The solvent used for all ICP-MS experiments was

**Scheme 1. Schematic Representation of the Solid-Phase Approach Used for the Synthesis of Conjugates 3 and 4**

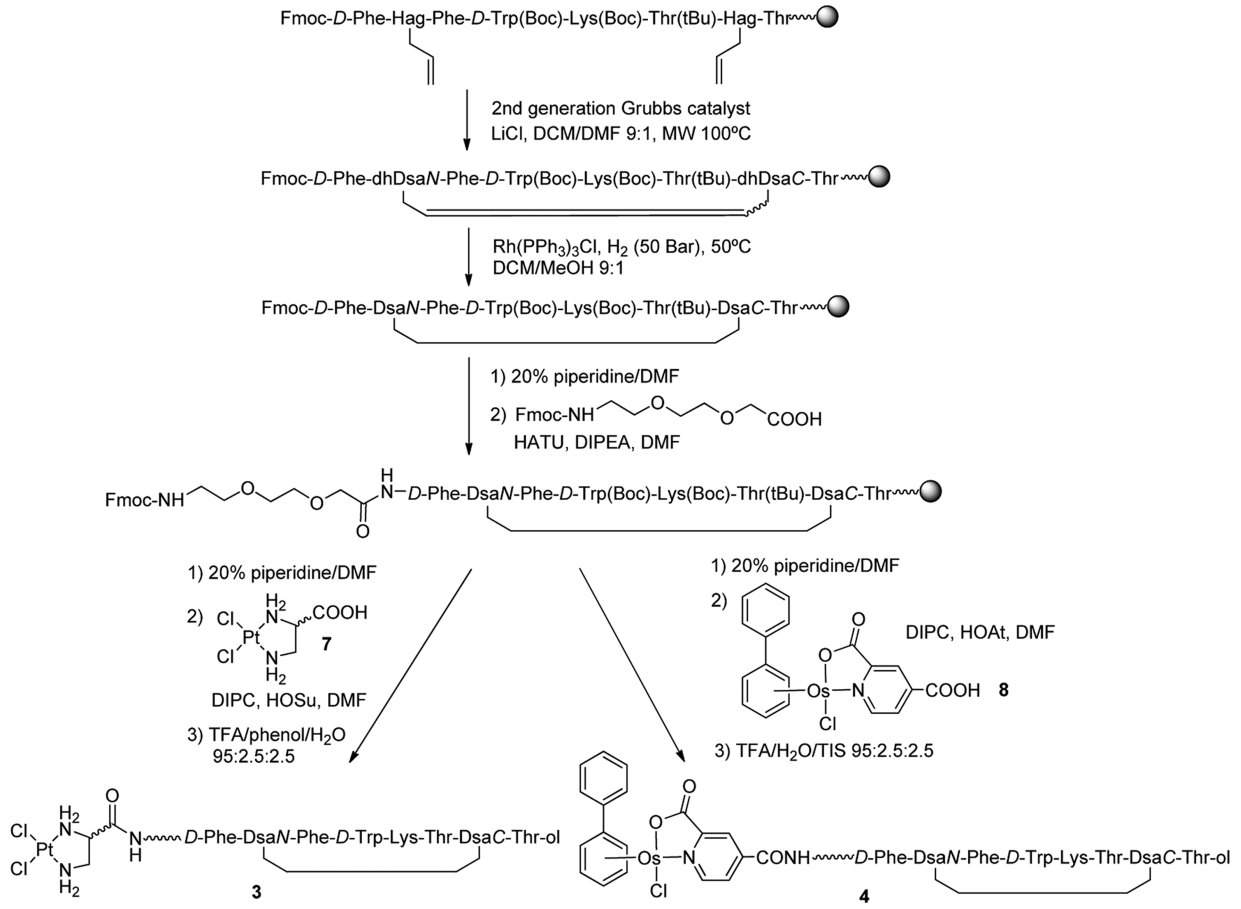


Milli-Q water with 1% $HNO_3$. The ruthenium standard (High-Purity Standards, 1000 $\mu$g/mL ± 5 $\mu$g/mL in 2% HCl) was diluted with Milli-Q water to 100 ppb. Ruthenium standards were freshly prepared in Milli-Q water with 1% $HNO_3$ before each experiment. The concentrations used for the calibration curve were in all cases 0, 1, 2, 5, and 10 ppb. The isotope detected was $^{101}$Ru and readings were made in triplicate. Rhodium was added as an internal standard at a concentration of 10 ppb in all samples.

**SSTR2 Expression Analysis.** SSTR2 expression on MCF-7, DU-145, and CHO cells surface was determined by double immunofluorescence. The cells were first fixed with PBS-1.5% formaldehyde and permeabilized with PBS-0.2%Tween 20 (Biorad). Then, the cells were incubated with a monoclonal antibody against human $sst_2$ receptor (R&D systems) during 30 min at 4 °C. After rinsing the cells with PBS, the cells were incubated 30 min at 4 °C in the presence of the Alexa-Fluor 488 conjugated goat antimouse IgG antibody (Invitrogen). Cells were washed again, and the fluorescence was analyzed using a flow cytometer (FACSCalibur, Becton Dickinson Immunocytometry Systems, San Jose, CA) equipped with the *CellQuest* software (Becton Dickinson). The fluorescence intensity of the cells was represented on a 4 orders of magnitude log scale (1−10 000). Ten thousand cells were analyzed in each experiment.

**Statistical Analysis.** The statistical analysis was performed with the *SPSS* statistical software for Windows (v 15.0; SPSS Inc., Chicago, IL, USA). Quantitative variables were expressed as mean and standard error (SE). The normality of the data was tested using the Kolmogorov−Smirnov test. The differences between data with normal distribution and homogeneous variances were analyzed using the parametric Student's *t* test. A value of $p < 0.05$ was considered significant.

## RESULTS AND DISCUSSION

**Synthesis and Characterization of Conjugates between a Dicarba Analogue of Octreotide and Dichloridoplatinum(II) and Osmium(II) Complexes.** In our previous work,[23] *cis*-dichlorido-(1-(carboxylic acid)-1,2-diaminoethane)platinum(II) complex, ([$PtCl_2$(dap)]), was chosen as a cisplatin analogue since it can form the expected intrachain Pt-*N*7/5′G,*N*7/3′G chelates upon reaction with DNA. The attachment of the platinum complex to the γ-aminoisobutyryl-derivatized dicarba analogue of octreotide (**2**) was carried out on a solid phase through the formation of an amide bond between its carboxylic function and the amine group of the spacer. Although the conjugate was able to bind to DNA in the same way as cisplatin, its low solubility in water precluded the evaluation of its biological activity. In order to improve the aqueous solubility for all the target conjugates, **3**−**6** (Chart 1), a poly(ethylene glycol) spacer has been introduced between the peptide sequence and the metal complex. This spacer is expected to be sufficiently long to keep the metal complex away from the pharmacophore sequence.

Following our previous results on the synthesis of platinum(II)−octreotide conjugates, a stepwise solid-phase strategy has been used for the preparation of conjugates **3**−**6**. This approach is particularly useful in this case, since it allows the


dx.doi.org/10.1021/bc300173h | *Bioconjugate Chem.* 2012, 23, 1838−1855

**Scheme 2. Schematic Representation of the Solid-Phase Approach Used for the Synthesis of Conjugates 5, 6, and 12**

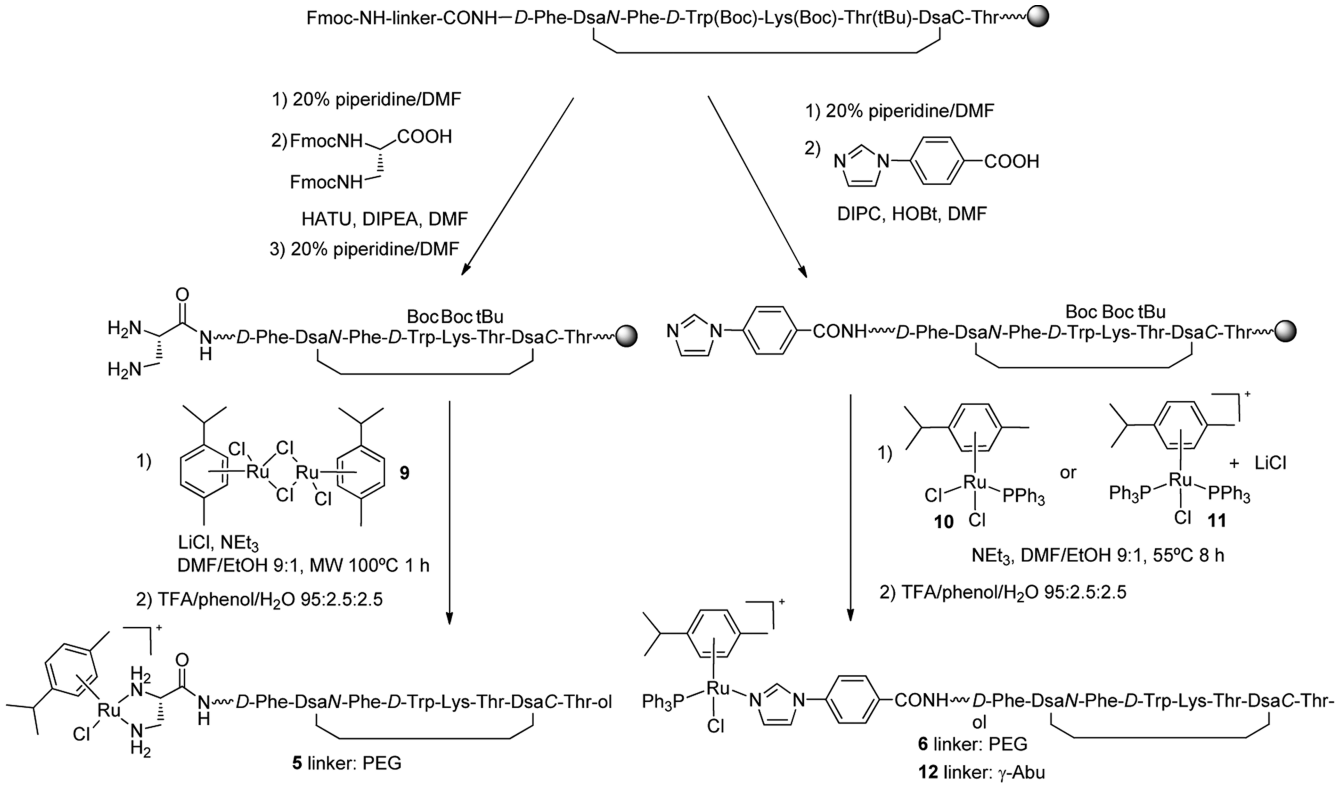


regioselective introduction of the metal complex at the *N*-terminal end of the cyclic peptide. Otherwise, in a solution-phase approach the $\varepsilon$-$NH_2$ of the Lys residue would compete with the *N*-terminal amino group of octreotide. In order to increase the stability of the metal−octreotide conjugates, the $CH_2$−$CH_2$ linkage has been chosen as a disulfide isoster, since this modification keeps a higher selectivity for $sst_2$ somatostatin receptor than the CH═CH linkage.[24]

First, the linear peptide was synthesized manually on a Rink amide resin-*p*-MBHA using standard Fmoc-*t*Bu methodology (Scheme 1). All suitably protected Fmoc-amino acids were incorporated with HATU in the presence of DIPEA in anhydrous DMF as a solvent. As previously described,[23,24] Fmoc-protected threoninol functionalized as the *p*-carboxybenzaldehyde acetal was first anchored to the solid support. In addition, the two cysteine amino acids in octreotide were replaced by allyl glycine residues to perform the cyclization reaction. Once the linear peptide precursor had been assembled, on-resin microwave-assisted ring-closing metathesis was carried out with second-generation Grubbs catalyst for 1 h at 100 °C. Then, hydrogenation of the double bond using Wilkinson's catalyst afforded the protected cyclic saturated dicarba analogue of octreotide (**2**) bound to the resin. Finally, an Fmoc-protected poly(ethylene glycol) linker, 8-(9-fluorenylmethyloxycarbonyl-amino)-3,6-dioxaoctanoic acid, was incorporated at the *N*-terminal end using HATU as a coupling reagent.

The final step involved the removal of the Fmoc protecting group of the spacer (20% piperidine in DMF) and the incorporation of the required metal complex onto the free amino function of the linker. For the synthesis of conjugate **3**, $[PtCl_2(dap)]$ (**7**) was coupled using DIPC and NHS in anhydrous DMF (15 h at rt, protected from light).[23] Cleavage from the resin and removal of the protecting groups were carried out by treatment with a TFA/phenol/$H_2O$ cocktail (95:2.5:2.5) for 1 h at rt. Reversed-phase HPLC analysis of the crude revealed a main double peak. Both peaks were isolated by semipreparative HPLC and characterized by HR MALDI-TOF and ESI MS and NMR as the expected diastereomeric dichloridoplatinum(II)−octreotide conjugates, **3**. The generation of both isomers is accounted from the use of a racemic platinum(II) complex.

Our next objective was focused on the conjugation of an organometallic osmium(II) complex to the dicarba analogue of octreotide. Among osmium complexes with anticancer activity, $[(\eta^6\text{-bip})Os(pico)Cl]$ is particularly interesting, since it exhibits promising activity in human ovarian cancer cells.[47,48] For this reason, we choose an analogue bearing a carboxylic function on the picolinate ligand, $[(\eta^6\text{-bip})Os(4\text{-}CO_2\text{-pico})Cl]$ (**8**), which would allow the attachment to octreotide. This complex has been very recently conjugated to polyarginines with different chain lengths using solid-phase procedures.[30] Hence, for the synthesis of conjugate **4**, $[(\eta^6\text{-bip})Os(4\text{-}CO_2\text{-pico})Cl]$ was coupled with either PyBOP or the more reactive HATU in the presence of DIPEA in anhydrous DMF (Scheme 1). After cleavage and deprotection with a TFA/TIS/$H_2O$ cocktail (95:2.5:2.5; 1 h at rt, protected from light), reversed-phase HPLC analysis revealed a main peak (30−40%), which was isolated and characterized by HR MS and NMR as the target conjugate **4**. The conversion yield was substantially increased (90%) when coupling was performed with DIPC and HOAt in anhydrous DMF for 3 h. It is important to mention that, during HPLC analysis of conjugate **4**, a less retained peak was always observed, which was characterized by MS as the aqua conjugate (substitution of Cl by $H_2O$). This result reveals fast hydrolysis


dx.doi.org/10.1021/bc300173h | *Bioconjugate Chem.* 2012, 23, 1838−1855

kinetics for this osmium(II) complex in comparison with that of the platinum(II) complex (see below).

**Synthesis and Characterization of Conjugates between a Dicarba Analogue of Octreotide and Ruthenium(II) Arene Complexes.** Ruthenium−octreotide conjugates, **5** and **6**, were synthesized on a solid-phase following a different strategy than that used for platinum and osmium conjugates (Scheme 2). Thus, instead of synthesizing the required ruthenium complexes bearing a carboxylic function, we decided to incorporate the appropriate ligand at the *N*-terminal end of the linker-derivatized peptide, which would allow the assembly of the organometallic ruthenium(II) complex around it. This approach avoids some of the difficulties found during the synthesis of carboxylic acid containing ruthenium complexes, and it could be applied to the parallel synthesis of libraries of ruthenium−peptide conjugates.

First, we focused on mononuclear ruthenium(II) arene complexes of the type $[(\eta^6\text{-arene})RuCl(XY)]^+$, where XY is a *N,N*-chelating ligand such as ethylenediamine. These compounds show high cytotoxicities both *in vitro* and *in vivo*, with $IC_{50}$ values comparable to carboplatin in human ovarian cancer cell lines (e.g., 9 $\mu$M for $[(\eta^6\text{-}p\text{-cym})RuCl(en)][PF_6]$).[49] In addition, they form monofunctional adducts at guanine nucleobases on DNA.

Attachment of $[(\eta^6\text{-}p\text{-cym})RuCl(en)]^+$ to octreotide was planned through the ethylenediamine ligand, as perfomed for the dichloridoplatinum(II) conjugate, which would lead to conjugate **5** (Chart 1). In order to incorporate 2,3-diaminopropionic acid into the *N*-terminal amino function of the linker-derivatized dicarba analogue of octreotide bound to the resin, the required $N^{\alpha}$,$N^{\beta}$-bis-(9-fluorenylmethyloxycarbonyl)-L-2,3-diaminopropionic acid was synthesized by reaction between L-2,3-diaminopropionic acid hydrochloride and 9-fluorenylmethyloxycarbonyl chloride. This Fmoc-protected chelating ligand was coupled with HATU in DMF in the presence of DIPEA for 1 h at rt (Scheme 2). After removal of the Fmoc protecting groups, the binding of the ruthenium arene to the chelating ligand was studied by reaction with the ruthenium dimer $[\{(\eta^6\text{-}p\text{-cym})Ru(\mu\text{-}Cl)Cl\}_2]$ (**9**). Optimized conditions required microwave irradiation at 100 °C for 1 h and the use of a slight excess of **9** (3 mol equiv) in the presence of LiCl (6.6 mol equiv) and $NEt_3$ (7.2 mol equiv) in a DCM/EtOH 9:1 mixture. The use of microwave irradiation in combination with this solvent was proven to be particularly important to achieve a good conversion yield. However, 30−40% conversion yields where obtained when DMF replaced DCM, and no irradiation was used (15 h heating at 60 °C). These results might be attributed to the instability of **9** at high temperatures during a prolonged time. Cleavage from the resin and deprotection was performed by treatment with a TFA/phenol/$H_2O$ cocktail (95:2.5:2.5) for 1 h at rt. Reversed-phase HPLC analysis of the crude revealed a main peak (65%) which was isolated by semipreparative HPLC and characterized by HR MALDI-TOF and ESI MS as the expected ruthenium−octreotide conjugate, **5**.

Once we had synthesized conjugate **5**, we explored the possibility of assembling mononuclear ruthenium(II) arene complexes through a single monodentate ligand incorporated into the peptide fragment instead of using chelating ligands. On the basis of the excellent antitumor activities of some ruthenium(II) three-legged "piano stool" complexes containing planar *N*-heteroaromatic $\sigma$-bonded ligands and phosphine ligands,[50] with $IC_{50}$ values lower than that of cisplatin, we focused on compounds of the type $[(\eta^6\text{-}p\text{-cym})RuCl(Im\text{-}Ph)(PPh_3)]^+$, where Im-Ph is 1-phenyl-imidazole. The conjugation of such triphenylphosphine-containing complexes to octreotide was planned through the phenyl ring linked to the imidazole ligand, which would allow the coordination of the ruthenium moiety. As in previous metal complexes, the hydrolysis of the Ru−Cl bond was expected to generate corresponding aqua species reactive toward DNA binding.

First, 4-(1*H*-imidazol-1-yl)benzoic acid was coupled onto two batches of linker-octreotide resin with DIPC and HOBt in anhydrous DMF for 1 h at rt, where linker refers to $\gamma$-aminoisobutyryl group or the poly(ethylene glycol) spacer (Scheme 2). The assembly of the metal complex was first explored with the $\gamma$-Abu linker-containing batch by using two ruthenium compounds, $[(\eta^6\text{-}p\text{-cym})RuCl_2(PPh_3)]$ (**10**) and $[(\eta^6\text{-}p\text{-cym})RuCl(PPh_3)_2]^+$ (**11**), since we hypothesized that the imidazole ligand could replace the more labile chlorido ligands. **10** was easily synthesized by refluxing dimer **9** with triphenylphosphine (2.3 mol equiv) in hexane for 15 h, whereas complex **11** was obtained from **10** by reaction with a slight excess of triphenylphosphine (2 mol equiv) in methanol at 35 °C for 2.5 h.[37,38]

Reaction of the imidazole-derivatized peptide-bound resin with complex **10** (4 mol equiv) was performed in the presence of $NEt_3$ (16 mol equiv) in a DMF/EtOH mixture (3:1) for 8 h at 55 °C. After treatment of the resin with a TFA/phenol/$H_2O$ cocktail (95:2.5:2.5), the desired conjugate **12** was detected in the crude (18%) together with the imidazole-derivatized octreotide (20%), as inferred by HPLC and MS analysis (Figure 1A).

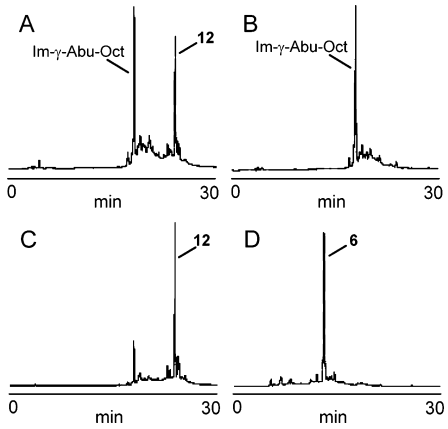


**Figure 1.** Reversed-phase HPLC traces of the reaction crudes for the synthesis of conjugate **12** by using complex **10** (A) or **11** (B) in the absence of LiCl or **11** in the presence of LiCl (C). Reaction crude for the synthesis of conjugate **6** when **11** was used in the presence of LiCl (D).

We next investigated the reaction of octreotide-bound resin with complex **11** under the same conditions. Unfortunately, reversed-HPLC analysis only revealed the presence of the imidazole-derivatized peptide, which indicates that imidazole was not able to substitute the chloride ligand in **11** (Figure 1B). This negative result might be attributed to the high steric hindrance around the metal because of the two bulky $PPh_3$ ligands. However, to our surprise, when the reaction of **11** (4 mol equiv) with the peptide was repeated in the presence of LiCl (4.4 mol equiv) and $NEt_3$ (16 mol equiv) in a DMF/EtOH 9:1 mixture for 8 h at 55 °C, HPLC analysis of the


dx.doi.org/10.1021/bc300173h | *Bioconjugate Chem.* 2012, 23, 1838−1855

cleaved, deprotected crude (TFA/phenol/$H_2O$ 95:2.5:2.5, 1 h rt) showed the presence of a main peak (57%) which was isolated and characterized by MS as conjugate **12** (Figure 1C). Hence, imidazole is able to replace one of the two $PPh_3$ ligands in **11** instead of the Cl ligand, thereby allowing the conversion yield of conjugate **12** to be improved in comparison with that obtained when complex **10** is used. As shown in Figure 1D, the assembly of the ruthenium complex by using these optimized conditions was almost quantitative onto the imidazole-derivatized octreotide resin that contains the poly(ethylene glycol) linker, which allowed the target conjugate **6** to obtain with high yield (Scheme 2). This compound was isolated by semipreparative HPLC and fully characterized by HR MS and NMR.

In order to gain insight into the mechanism of this reaction, complex **11** was mixed with LiCl (1.4 mol equiv) and $NEt_3$ (1.9 mol equiv) in anhydrous DMF and heated at 55 °C. As shown in the $^{31}P$ NMR spectra (Figure 2), the single chemical shift

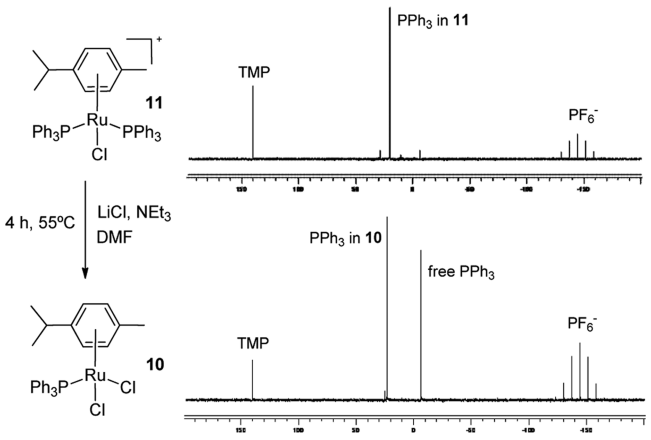


**Figure 2.** Schematic representation of the transformation of complex **11** to **10** (left) and $^{31}P$ NMR spectra of **11** (A) and of the reaction crude after heating **11** in the presence of LiCl and $NEt_3$ for 4 h at 55 °C (B).

corresponding to the two $PPh_3$ ligands in **11** ($\delta$: 20.0 ppm) disappeared after 4 h. The two new signals ($\delta$: 23.2 and −6.4 ppm) were assigned to the $PPh_3$ ligand in complex **10** and to the released $PPh_3$, respectively. These results demonstrate the *in situ* generation of complex **10** from **11** because of the presence of LiCl. This reaction might have future applications in the synthesis of new ruthenium complexes for catalysis or biomedical applications.

**Activation of Metal−Octreotide Conjugates by Aqueous Hydrolysis.** In general, the cytotoxic activity of metal-based anticancer drugs is intimately related with the processes that mediate their activation in aqueous media; these processes are known to facilitate the interaction of the metal, its ligands or the complex, or a fragment with the biological target (e.g., DNA, RNA, or proteins). In addition, aqueous stability is another fundamental prerequisite, since it might condition their success in clinical development. Cisplatin and its analogues can be considered prodrugs since their activation is produced through the dissociation of anionic ligands.[22,51] The resulting positively charged aqua species coordinate strongly to nuclear DNA while neutral complexes do not, which demonstrates that in these family of compounds the metal plays a functional role.[22] Organometallic complexes containing a labile group prone to substitution can also be activated inside the cells through hydrolysis. As previously stated, the activation of piano-stool organometallic ruthenium(II) complexes of the type $[(\eta^6\text{-arene})RuCl(XY)]^+$, where XY is a neutral chelating ligand, proceeds through the release of chloride ligand. The resulting aqua species is responsible for ruthenation of DNA by generating monofunctional adducts on guanine nucleobases. In a similar manner to cisplatin and related platinum(II) compounds, the high extracellular chloride concentration (100 mM) in comparison with that present in the nucleus and cytoplasm (4 and 22.7 mM, respectively)[52] ensures that the intact drug reaches its biological target before activation takes place. In addition, a close correlation between cancer cell cytotoxic activity and the capacity of some ruthenium(II) arene complexes to undergo hydrolysis of the Ru-halide bond has been established.[53] Osmium(II) arene complexes containing *N,N*-chelating ligands, such as ethylenediamine, experience much slower ligand exchange kinetics than ruthenium analogues.[54] The higher acidity of the water molecule bound to the osmium at physiological pH makes these compounds exist largely in their less reactive hydroxido form. These problems have been solved by using picolinate as chelating ligand since it increases both the hydrolysis rate and the basicity of the water molecule in the aqua species (e.g., $[(\eta^6\text{-arene})Os(pico)Cl]$) and, for instance, generates compounds with similar anticancer activity as ruthenium-arene analogues.[36,47]

On the basis to these precedents, we wanted to assess whether hydrolysis of the M-Cl bond occurs when Pt, Ru, and Os complexes are conjugated to octreotide. The stability of conjugates **3**−**6** (Chart 1) was investigated in aqueous solution at different chloride concentrations mimicking typical blood plasma, cell cytoplasm, and cell nucleus (100, 22.7, and 4 mM, respectively). In all cases, metal−octreotide conjugates (10 $\mu$M) were incubated at 37 °C for 24 h. In general, HPLC analysis showed that the peak of the parent chloride compound (e.g., $R_t$ = 20.3 min for conjugate **4**) evolved into a new less retained peak ($R_t$ = 16.9 min), which was isolated and characterized by ESI MS as the aqua conjugate (substitution of Cl by $H_2O$).

As previously found in some osmium(II) complexes,[48] the hydrolysis extent of conjugate **4** was highly dependent on the NaCl concentration. Almost 95% of the conjugate was hydrolyzed in the 4 mM NaCl solution, but the hydrolysis was substantially decreased in the more concentrated solutions of NaCl (Table 1). These results indicate that the covalent attachment of the peptide does not interfere with the hydrolysis properties of this osmium complex and,[48] more importantly, that the aqua species is not deactivated by reaction with amino

**Table 1. Percentage of Aqua Adduct Formation in Water at Chloride Levels Typical of Blood Plasma (100 mM), Cell Cytoplasm (22.7 mM), and Cell Nucleus (4 mM), and Percentage of the Conjugate−DNA Adduct Formation in Aqueous 4 mM NaCl**

| | % aqua adduct | | | % DNA adduct |
|---|---|---|---|---|
| conjugate | 4 mM NaCl | 22.7 mM NaCl | 100 mM NaCl | 4 mM NaCl |
| **3** | 16 | 7 | 3 | 42 |
| **4** | 95 | 35 | 12 | 49 |
| **5a**[a] | 97 | 83 | 74 | 37 |
| **6** | 0 | 0 | 0 | 0 |

[a]See the experimental section.


dx.doi.org/10.1021/bc300173h | *Bioconjugate Chem.* 2012, 23, 1838−1855

acids from the carrier peptide. Similar results were obtained for the ruthenium conjugate **5** at the 4 mM chloride concentration. However, the extent of hydrolysis of the Ru−Cl bond was substantially decreased at the higher NaCl concentrations (Table 1).

Regarding conjugate **3**, the hydrolysis of the Pt−Cl bond occurred to a lower extent than for conjugates **4** and **5** (only 16% after 24 h in 4 mM NaCl solution), and it was almost abolished at higher chloride concentration.

On basis to these results, it is expected that octreotide in conjugates **3** and **4** will have a positive effect on the delivery of the less reactive intact prodrug while outside the cell, but once in the cell cytoplasm and, particularly, in the cell nucleus, Pt and Os complexes will be selectively activated through hydrolysis to generate a species reactive toward DNA binding. However, hydrolysis of conjugate **5** in the blood plasma and in the cell cytoplasm might have important consequences for its biological activity since the metal complex could be deactivated by reaction with other potential ligands such as peptides or proteins.

To our surprise, no hydrolysis occurred in the case of conjugate **6** upon incubation for 24 h at 37 °C, as inferred by HPLC analysis together with MS (see below).

**DNA Binding Studies.** In general, the chlorido species of Pt(II), Ru(II), and Os(II) complexes are relatively less reactive toward DNA nucleobases in comparison with the aqua adducts. The chloride concentration in the nucleus of cells (*ca.* 4 mM) is much less than that in the cytoplasm (*ca.* 22.7 mM) or outside cells (*ca.* 100 mM), which favors the formation of reactive aqua adducts in the vicinity of DNA. We incubated conjugates **3**−**6** in 4 mM NaCl at 37 °C with the short DNA oligonucleotide, 5′dCATGGCT. This oligonucleotide contains the target GG sequence of the anticancer drug cisplatin and is known to give the expected platinum 1,2-intrastrand GG chelates upon reaction with cisplatin, [Pt(en)$Cl_2$], or a dichloridoplatinum(II) conjugate of a dicarba analogue of octreotide.[23,41]

In the case of the platinum conjugate **3**, HPLC analysis showed the formation of a new peak with higher retention time than the parent oligonucleotide (42% after 24 h; see Table 1), attributable to the hydrophobicity of the platinum−peptide fragment. This new product was isolated and characterized by HR MALDI-TOF MS as an adduct between **3** and 5′dCATGGCT in which both chloride ligands had been lost. As expected from previous results,[23] MS analysis after enzymatic digestion with 5′- and 3′-exonucleases (bovine spleen and snake venom phosphodiesterases, respectively)[42,43] revealed the formation of a chelate between the platinum fragment of the conjugate and both guanines of the DNA chain (Scheme 3).

When osmium− and ruthenium(dap)−octreotide conjugates were incubated with 5′dCATGGCT, a major monofunctional adduct was formed between the metal fragment of the conjugate and the DNA chain. In both cases, the high metalation yield (49% for **4** and 37% for **5**) is in good agreement with the high degree of hydrolysis of the Os/Ru−Cl bonds. Enzymatic digestion in combination with MS revealed that in both cases metalation occurred at the guanine in the 5′ position (G4, see Scheme 3). This is a similar trend to that previously found with monofunctional platinum(II) complexes, such as $\{Pt(dien)\}^{2+}$, since they react exclusively with the 5′G nucleobase in the 5′dCATGGCT sequence.[41] The high affinity of similar ruthenium(II) arene complexes, such as [($\eta^6$-*p*-cym)RuCl(en)]$^+$ or [($\eta^6$-benzene)Ru(en)($OH_2$)]$^{2+}$, for the *N*7 position of guanine over the other DNA nucleobases has been observed previously.[55−57] Regarding organometallic osmium(II) complexes with picolinate ligands, such as [($\eta^6$-biphenyl)Os(picolinate)Cl]$^+$, rapid binding to calf thymus DNA has also been found.[58]

**Scheme 3. Formation of Adducts between Conjugates 3−5 and the Oligonucleotide**

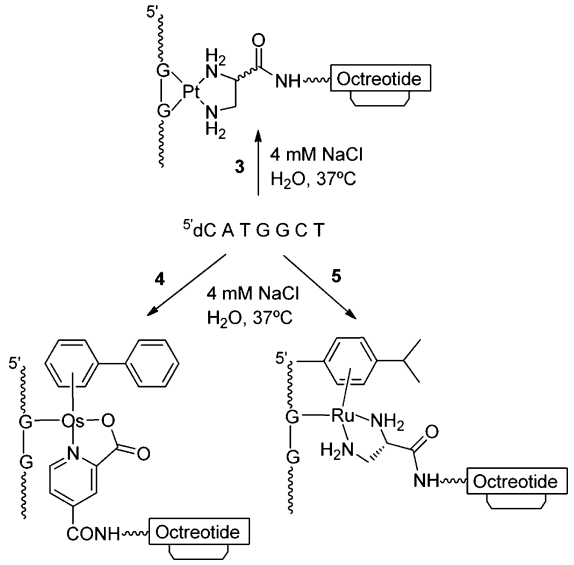


Finally, the reaction of the ruthenium−octreotide conjugate **6** with DNA was studied. In good agreement with the absence of hydrolysis of the Ru−Cl bond in this compound, ruthenation of 5′dCATGGCT was not observed even after 48 h.

The overall results demonstrate that the activation of the M-Cl bond through hydrolysis in the Ru and Os conjugates seems to be very important for the binding to DNA, and there is a strong preference for the guanine nucleobases, especially those located at the 5′ end in GG sequences. However, in the case of the Pt(dap)-octreotide conjugate, platination is observed despite the slow kinetics for the hydrolysis of the Pt−Cl bond in the low chloride medium as found in the nucleus. The high thermodynamic stability of the *N*7,*N*7-GG intrastrand adduct might account for this result.

**Efficiency of Intracellular Delivery of Dicarba Analogue of Octreotide (2).** Compared to octreotide (**1**), the binding affinity of the dicarba analogue of octreotide (**2**) (Chart 1) is slightly reduced for $sst_2$, $sst_4$, and $sst_5$ receptors, although this reduction is smaller in the case of $sst_2$ receptor (about 23-fold for $sst_2$ vs 36- and 48-fold for $sst_4$ and $sst_5$, respectively).[6,24] However, as previously stated, this high affinity toward $sst_2$ receptor (44 nM) still makes **2** a suitable stabilized analogue of somatostatin to deliver cytotoxic metal complexes into cancer cells. In order to check the capacity of internalization of analogue **2** in our cell lines by confocal microscopy and flow cytometry, we labeled it with fluorescein. For the synthesis of the fluorescein-labeled dicarba analogue of octreotide (**13**), 5(6)-carboxyfluorescein was coupled on the linker derivatized peptide-bound resin by using DIPC and HOAt as coupling reagents. Washings with 20% piperidine/DMF before the final acidic treatment yielded a highly pure peptide.[59] As a control, fluorescein-labeled octreotide (**14**) was also synthesized using solid-phase procedures.

Next, the internalization capacity of analogue **2** was determined by confocal microscopy, after the incubation of


dx.doi.org/10.1021/bc300173h | *Bioconjugate Chem.* 2012, 23, 1838−1855

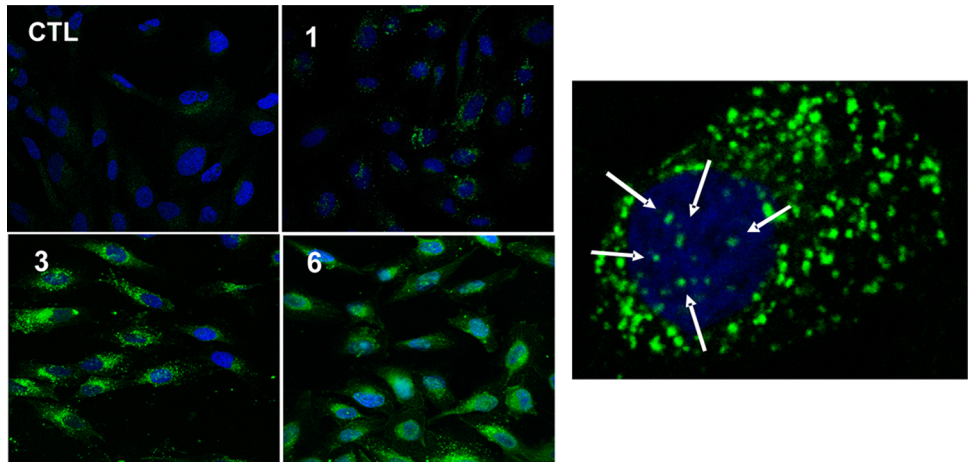


**Figure 3.** Confocal microscopic imaging of the internalization of the fluorescein-labeled dicarba analogue of octreotide (**13**) in MCF-7 cells. Left: MCF-7 cells incubated with 50 $\mu$M of **13** for 1, 3, and 6 h at 37 °C or medium alone as a control (CTL). The cell nuclei were stained with Hoechst (blue). The localization of **13** is indicated by the green fluorescence. Right: Higher-magnification image (1000×) of a MCF-7 cell incubated with 50 $\mu$M of **13** for 3 h at 37 °C. Arrows indicate the nuclear localization of **13**.

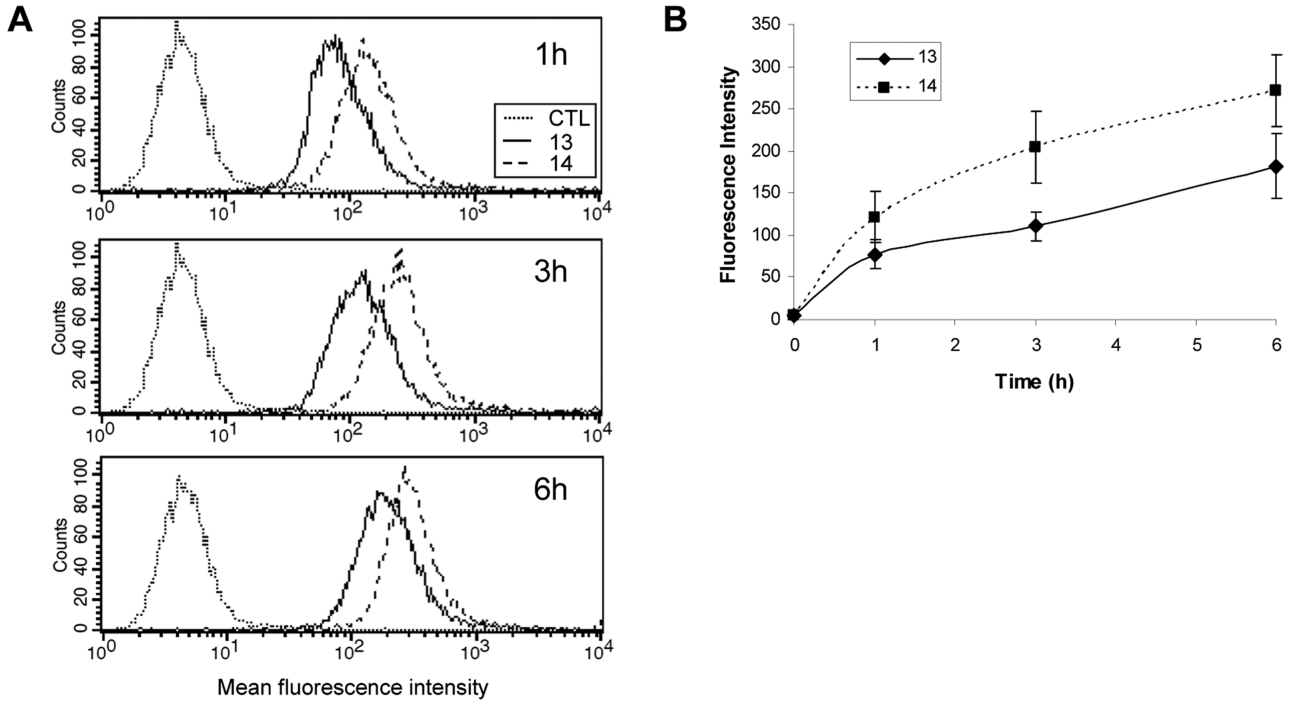


**Figure 4.** Intracellular delivery efficiencies of fluorescein-labeled dicarba analogue of octreotide (**13**) and of fluorescein-labeled octreotide (**14**) in MCF-7 cells. MCF-7 cells were incubated with the peptides for 1, 3, and 6 h at 37 °C or medium alone (CTL). The fluorescence intensity of the cells, corresponding to the intracellular uptake of the peptides, was determined by flow cytometry. (A) Flow cytometry histograms representing the fluorescence intensity of 10 000 cells on a four-decade log scale. Peptides **13** and **14** are depicted by solid and dashed lines, respectively. (B) Kinetics of the cellular uptake of **13** and **14**. Each point in the graphs represents the mean intracellular fluorescence intensity of three independent experiments ± SE.

sstr$_2$-expressing human breast cancer MCF-7 cells with 50 $\mu$M of the corresponding fluorescein-labeled peptide (**13**) for different times (1, 3, and 6 h). After 1 h of treatment, fluorescent vesicles, most likely endosomes, were visible in the cytoplasm of most of the examined cells, confirming the cellular uptake of the peptide (Figure 3). After 3 and 6 h, the number and the fluorescence density of the vesicles markedly increased, revealing an intense internalization of **13** during this period of time. At these time points, the vesicles were mainly clustered at the periphery of the cell nucleus. Higher-magnification (1000×) images from cells exposed to **13** for 3 h (Figure 3) revealed that, although the fluorescence vesicles were located mainly in the cell cytoplasm, a small proportion of the fluorescence was localized within the cell nucleus. Some authors have reported that somatostatin ligands may accumulate in the cell nucleus,[60,61] although the pathway for their nuclear localization remains to be elucidated.

The qualitative observations in confocal microscopy studies were confirmed with quantitative data obtained by flow cytometry. As represented in Figure 4A, the mean intracellular fluorescence intensity, corresponding to the internalization of **13**, increased over time. The intracellular fluorescence intensity

increased from 78 ± 16 at 1 h to 111 ± 17 at 3 h and 182 ± 39 at 6 h confirming an active cellular uptake of the peptide at these time points. In order to evaluate if **13** internalizes to a similar extent as native octreotide, MCF-7 cells were incubated in parallel with **14**. As expected from the higher affinity of octreotide for the somatostatin receptors,[6,24] the intracellular uptake of **14** was more elevated, by 40−57%, compared with that obtained in cells incubated with **13**. As shown in Figure 4B, the internalization kinetics was parallel for both peptides and it is also in good agreement with previous reports.[62,63] Despite the differences in the amount of internalized peptide, these results demonstrate that the dicarba analogue of octreotide (**2**) displays the internalization properties required to deliver the cytotoxic metal complexes into cancer cells.

**Cancer Cell Cytotoxicity.** To estimate the *in vitro* antitumor potential of the conjugates **3**, **4**, **5**, and **6**, their antiproliferative activity was determined in the MCF-7 cell line. The compounds were screened at a wide range of concentrations (from 0 to 250 $\mu$M) to determine the concentration that inhibits the cell growth by 50% ($IC_{50}$). The conjugates that did not inhibit cell growth by more than 50% at 250 $\mu$M were considered to be inactive. As shown in Table 2, only conjugate **6** displayed a measurable antiproliferative activity, and even that was only moderate ($IC_{50}$ = 63.00 ± 1.53). On the basis of these results, we wondered whether the cytotoxic activity might be a consequence of the metal complex itself or of the conjugation to the peptide moiety. Hence, we tested the cytotoxicity of the parent metal complex alone, including the ligand attached to the peptide. The following complexes were synthesized and used as controls (Chart 2): [$PtCl_2$(Etdap)] (**15**), [($\eta^6$-*p*-cym)RuCl(dap)]$^+$ (**16**), and [($\eta^6$-*p*-cym)RuCl(Im-BzCOOMe)($PPh_3$)]$^+$ (**17**). Although we planned to mask the carboxylic function in all the complexes as a methyl or ethyl ester to avoid a negative charge that might hinder cell uptake and lower their biological activity, the complex [($\eta^6$-*p*-cym)RuCl(Etdap)]$^+$ spontaneously hydrolyzed to **16** during the workup of the reaction. Regarding the osmium complex [($\eta^6$-bip)OsCl(4-$CO_2$Et-pico)Cl)]$^+$ (**18**), a moderate cytotoxic activity in the human ovarian A2780 and A2780cis cell lines ($IC_{50}$ = 44 and 61 $\mu$M, respectively) has been recently reported in comparison with that of [($\eta^6$-bip)OsCl(4-Me-pico)Cl)]$^+$ ($IC_{50}$ = 4.4 and 7.6 $\mu$M in the A2780 and A2780cis cell lines, respectively).[36] Cytoxicity assays of the control complexes revealed that **17** was highly effective in MCF-7 cells, displaying an $IC_{50}$ value (3.32 ± 0.54) comparable to that of cisplatin in this cell line ($IC_{50}$ = 3.04 ± 0.25). In contrast, a moderate antiproliferative activity was obtained for complex **15** ($IC_{50}$ = 67.00 ± 19.01) while complex **16** was noncytotoxic (Table 2).

**Table 2. $IC_{50}$ Values of Conjugates 3−6 and Control Complexes 15−17 in MCF-7 Cells**[a]

| | $IC_{50}$ ($\mu$M) | | | |
|---|---|---|---|---|
| Conjugates | **3** | **4** | **5** | **6** |
| | >250 | >250 | >250 | 63.00 ± 1.53 |
| Complexes | **15** | - | **16** | **17** |
| | 67.00 ± 19.01 | - | >250 | 3.32 ± 0.54 |

[a] $IC_{50}$: Inhibitory concentration that reduce by 50% the cell viability. The cytotoxicity was determined by the MTT assay after 72 h of drug exposure. Data represents the mean ± SE of at least three independent experiments.

Two important conclusions can be drawn from these results. First, high cytotoxic activity of the metal complex itself seems to be crucial for the efficacy of the conjugates as antitumoral agents. Second, conjugation of the complexes to the peptide moiety diminishes their cytotoxic capacity. For example, the cytotoxic activity of the ruthenium(II) arene complex [($\eta^6$-*p*-cym)RuCl(Im-BzCOOMe)($PPh_3$)]$^+$ (**17**) is reduced about 19-fold when conjugated to the octreotide analogue (**6**), whereas complexes with moderate activity, such as [$PtCl_2$(Etdap)] (**15**) or [($\eta^6$-bip)OsCl(4-$CO_2$Et-pico)Cl)]$^+$ (**16**),[36] afford inactive peptide conjugates (**3** and **4**, respectively). On the other hand, the lack of activity for complex [($\eta^6$-*p*-cym)RuCl(dap)]$^+$ (**16**) or its octreotide conjugate (**5**) might be attributable to the high hydrolysis rate of the Ru−Cl bond, which would cause deactivation of the activated species by reaction with other biomolecules before it reaches nuclear DNA.

It is also interesting that the only conjugate that displays cytotoxic activity (**6**) does not interact with DNA, which can be attributed to the absence of hydrolysis of the Ru−Cl bond, even at a low chloride concentration (4 mM). This is also consistent with the fact that control complex **17** does not interact with double-stranded plasmid DNA after 48 h of incubation, as determined by electrophoretic mobility experiments (see Figure S-18 in the Supporting Information). Similarly to conjugate **6**, the aqua adduct of complex **17** was only formed after overnight incubation with a large excess of $AgNO_3$, as inferred by $^1$H and $^{31}$P NMR (see the Supporting Information). The overall results suggest that the cytotoxic activity of **6** and **17** might not be a consequence of their coordination to *N*-donor ligands from nucleic acids (DNA or RNA) or proteins. However, it cannot be rule out that their activation under physiological conditions occurs through coordination to sulfur-containing amino acids in peptides such as glutathione or in proteins.

In order to gain insight into the implication of somatostatin subtype-2 receptor on the cytotoxic activity of the ruthenium−octreotide conjugate **6**, the cellular uptake of this compound was compared with that of the unconjugated ruthenium complex **17**. Ruthenium accumulation (determined here as the net effect of influx and efflux of Ru) in the MCF-7 cancer cell line was determined by ICP-MS after a 24 h exposure to the compounds. Interestingly, the intracellular level of ruthenium after exposure to conjugate **6** (143.14 ± 16.6

**Chart 2. Structures of the Control Metal Complexes**

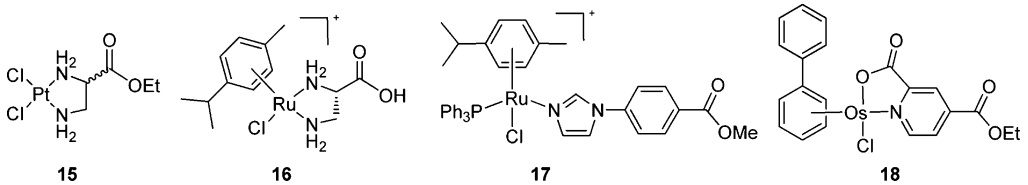



dx.doi.org/10.1021/bc300173h | *Bioconjugate Chem.* 2012, 23, 1838−1855

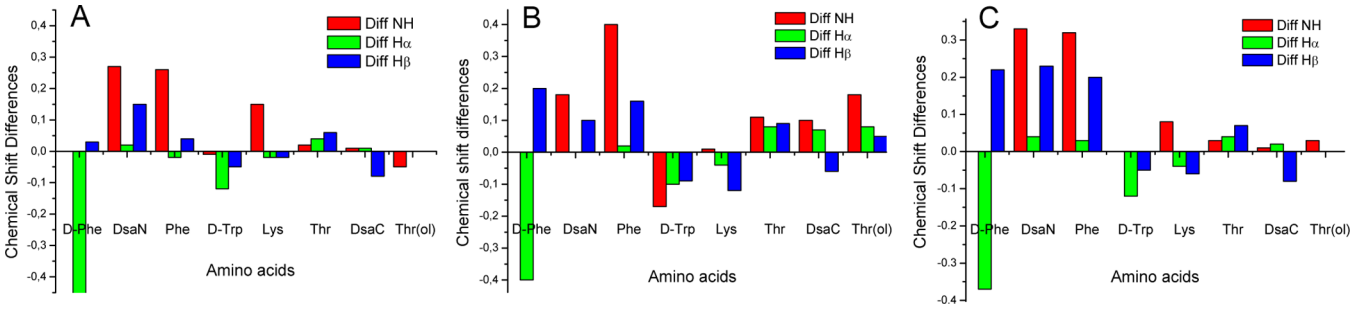


**Figure 5.** Chemical shift differences for NH, H$\alpha$, and H$\beta$ protons between conjugates **3** (A), **4** (B), and **6** (C) and the dicarba analogue of octreotide (**2**).[24]

pmol Ru/$10^6$ cells) was higher than that of the parent complex **17** (68.01 ± 2.2 pmol Ru/$10^6$ cells). Such a significant difference between these compounds reveals that conjugation to the peptide moiety has a positive effect on the internalization of the ruthenium complex, thereby suggesting that the attachment of the metal complex to the peptide does not disturb its active conformation and hence its affinity toward somatostatin receptors is maintained (see below). Although the covalent attachment of a potential metal-based drug to a receptor-binding peptide such as octreotide is expected to increase the bioavailability, delivery, and accumulation of the complex to cancer cells, it must also be borne in mind that the peptide moiety might also inhibit or weaken the interaction of the metal fragment with the final biological target (e.g., DNA, RNA, or proteins), which would compromise its cytotoxic activity.[25] Release of the ruthenium fragment from the conjugate might be necessary to allow it to reach its target site. This might explain the apparently contradictory results from cytotoxicity and cellular uptake studies, since in this case, the covalent attachment of the ruthenium complex to the dicarba analogue of octreotide **2** increases uptake and accumulation of the drug in the cancer cell while the cytotoxic activity of the final conjugate is reduced.

**Conformational Analysis by NMR Spectroscopy.** It is well-known from NMR studies in water and in DMSO-$d_6$ solution that octreotide (**1**) adopts a predominant type II′ $\beta$-turn conformation across residues Phe$^7$-*D*-Trp$^8$-Lys$^9$-Thr$^{10}$.[64,65] The stability of this conformation together with the orientation of exocyclic residues (*D*-Phe$^2$ and Thr-ol$^{15}$) plays an important role in the binding of octreotide and its analogues to somatostatin receptors.[66,67] Regarding the dicarba analogue of octreotide used in this work (**2**), D′Addona et al. have recently described that replacement of cystine by a $CH_2$−$CH_2$ linkage does not substantially alter the secondary structure in the active region.[24] These NMR studies also suggest that there exists a conformational equilibrium between the antiparallel $\beta$-sheet structural cluster and a second conformational ensemble involving folded structures for the *C*-terminal residues. This hypothesis is in good agreement with previously reported findings for **1** that indicate that *C*-terminal amino acids fold into a $3_{10}$-helix-like array or in a similar helical ensemble.[66] Furthermore, it is important to consider that the structure of **2** in the region of the *N*-terminal *D*-Phe$^2$ and *C*-terminal Thr(ol)$^{15}$ is significantly different from that previously reported for **1**,[66] which might explain the differences in affinity for somatostatin receptors.[24] Given the implication of these amino acids both in the affinity and in the specificity for somatostatin receptors, we investigated whether the covalent attachment of metal complexes to the *N*-terminal end of **2** through a poly(ethylene glycol) linker might alter the active conformation of the peptide and, in particular, the structure around *D*-Phe$^2$ and Thr-ol$^{15}$.

In order to gain some insight into peptide conformation, conjugates **3**, **4**, and **6** were studied by 1D and 2D $^1$H NMR spectroscopy. In all conjugates, significant line-broadening was observed at conjugate concentrations above 1 mM, suggesting that oligomerization takes place under these conditions. This effect is specially pronounced in the case of the osmium−octreotide conjugate (see the Supporting Information). To avoid oligomerization, 2D NMR spectra were recorded at a peptide concentration of 0.8 mM. Signals of the peptide were completely assigned using standard techniques (see Tables S1−3 in the Supporting Information). Resonances of the linker and of ligands in the metal fragments were also indentified, although not all of them could be unambiguously assigned to specific protons.

A comparison between the chemical shifts of the peptide fragment in the conjugates and the dicarba-analogue of octreotide (**2**)[24] indicates that residues *D*-Trp$^8$-Lys$^9$-Thr$^{10}$-DsaC$^{14}$-Thr(ol)$^{15}$ have very similar chemical shifts, whereas significant differences are observed for protons of the amino acids *D*-Phe$^2$-DsaN$^3$-Phe$^7$ (Figure 5). This suggests that the peptide structure is only affected in the latter region. The chemical shift of H$\alpha$ of *D*-Phe$^2$ is notably shifted downfield. This shift is attributed to the covalent attachment of the linker to the $\alpha$-amino group of this amino acid through an amide bond. Interestingly, peaks for the NH protons of DsaN$^3$ and Phe$^7$ amino acids in all conjugates (and to a lesser extent for the H$\beta$ signals) were shifted upfield.

Molecular dynamics calculations were carried out to gain further insight in the structural alterations induced in the peptide structure by the covalent attachment of the metal complex. The results are illustrated in Figure 6. The peptide backbone is not significantly altered with respect to the structure of the dicarba analogue of octreotide (**2**). In particular, the $\beta$-turn backbone geometry around residues *D*-Trp$^8$-Lys$^9$-Thr$^{10}$-DsaC$^{14}$-Thr(ol)$^{15}$ is totally preserved. The main changes occur in residues *D*-Phe$^2$ and DsaN$^3$. Side chain conformations are less defined than in **2**. Linker and ligand fragments are mainly disordered. In some of the calculated conformers, the ligand or the linker exhibits contacts with aromatic residues *D*-Phe$^2$ and Phe$^7$ as well as with DsaN$^3$ (see Figure 6). These residues correspond to those that have changes in their $^1$H NMR chemical shifts with respect to the unmodified peptide. This is also in good agreement with the fact that some NOEs were observed between the linker and *D*-Phe$^2$ (see Figure S-20 in the Supporting Information).


dx.doi.org/10.1021/bc300173h | *Bioconjugate Chem.* 2012, 23, 1838−1855

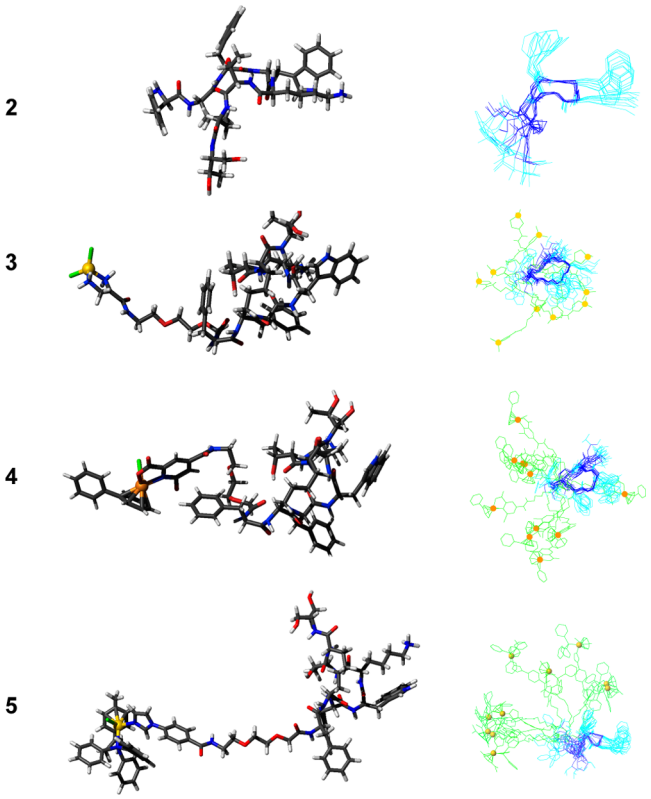


**Figure 6.** Model structures of the dicarba analogue of octreotide (**2**) and of conjugates **3**, **4**, and **6** (see Chart 1). Left: representative conformer. Right: ensemble with 10 conformers resulting from molecular dynamics calculations. Superposition was done by fitting the backbone peptide heavy atoms.

The NMR data and molecular dynamics calculations suggest that the covalent attachment of the metal complex does not substantially alter the global structure of the peptide. However, the aromatic ligands of the ruthenium and osmium complex in conjugates **4** and **6**, as well as the linker appear to have a tendency to interact with the aromatic residues located to their near side of the peptide sequence, which could be favored by the high flexibility of the poly(ethylene glycol) linker. This is particularly important in the case of the $Phe^7$ residue, since this amino acid is included in the so-called pharmacophore sequence of octreotide. These results support the hypothesis that the covalent attachment of both fragments might generate a significant population of peptide conformations with a decreased affinity for somatostatin receptors in comparison with that of the dicarba analogue of octreotide **2**. However, the dicarba analogue of octreotide **2** still retains the ability to internalize metal complexes upon conjugation, as demonstrated cellular uptake experiments with **6** and **17**.

**Selectivity of the Ruthenium–Octreotide Conjugate (6).** The main objective of a targeted strategy is the selective delivery of a cytotoxic drug to cancer cells in order to reduce toxicity to normal cells. Consequently, the reduction of the antiproliferative activity of a metal complex when conjugated with octreotide (Table 2) could be compensated by a selective and a more efficient delivery of the compound to the targeted cells. In order to corroborate this hypothesis, we determined whether the conjugation of the ruthenium(II) arene complex **17** to the octreotide analogue **2** (conjugate **6**) is correlated with its vehiculization to tumor cells overexpressing $sstr_2$, the most relevant receptor for octreotide internalization.[68] To this end, we further analyzed the cytotoxic activity of conjugate **6** in human prostate tumor DU-145 cells as well as and in the Chinese hamster ovary (CHO) cell line, in order to assess the selectivity of the ruthenium–octreotide conjugate for cancer cells with respect to normal cells (Table 3). As shown in Figure 7A, DU-145 cells were markedly more responsive to **6** than the MCF-7 and CHO cells, as the $IC_{50}$ value (26.00 ± 3.46) was 2.4-fold lower than in MCF-7 cells and about 1.7-fold lower than in CHO cells ($IC_{50}$: 45.17 ± 2.61) (Table 3). This difference in the cytotoxic activity of conjugate **6** between the cell lines cannot be attributed to a different activity of the metal fragment in the different cells, as the control complex **17** cytotoxicity was higher in MCF-7 ($IC_{50}$ = 3.32 ± 0.54) and

**Table 3. $IC_{50}$ Values of the Ruthenium–Octreotide Conjugate 6 and Control Complex 17 in Human Cancer Cell Lines (MCF-7 and DU-145) and in Normal Cells (CHO)[a]**

| | cell line, $IC_{50}$ ($\mu$M) | | |
|---|---|---|---|
| compound | MCF-7 | DU-145 | CHO |
| **6** | 63.00 ± 1.53 | 26.00 ± 2.00 | 45.17 ± 2.61 |
| **17** | 3.32 ± 0.54 | 6.80 ± 0.99 | 5.8 ± 0.01 |

[a]$IC_{50}$: Inhibitory concentration that reduce by 50% the cell viability. The cytotoxicity was determined by the MTT assay after 72 h of drug exposure. Data represents the mean ± SE of at least three independent experiments.

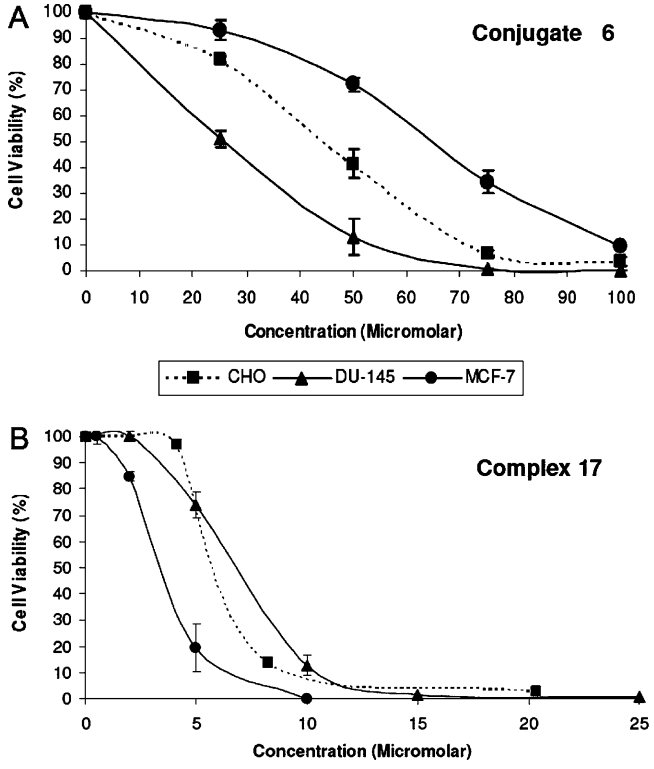


**Figure 7.** Cytotoxic effect of conjugate **6** (A) and complex **17** (B) in the MCF-7, DU-145, and CHO cell lines. Cells were treated for 72 h with the indicated concentrations of each compound. The cell viability was determined using the MTT assay. Each point in the graphs represents the mean of three independent experiments ± SE.


dx.doi.org/10.1021/bc300173h | *Bioconjugate Chem.* 2012, 23, 1838–1855

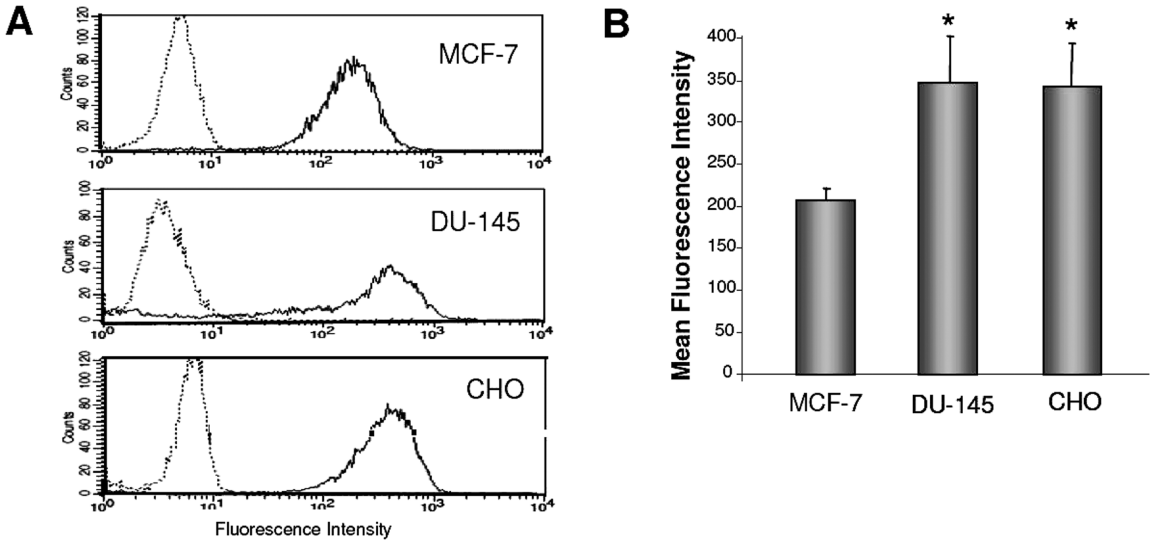


**Figure 8.** Expression of the $sst_2$ receptor on MCF-7, DU-145, and CHO cell lines. (A) Representative flow cytometry histograms obtained after the indirect immunofluorescence staining of the cells. Solid lines represent the fluorescence intensity of the cells after the incubation with an antibody against $sstr_2$ together with a control secondary antibody. Dotted lines indicate the background staining with the secondary antibody alone. (B) Each column in the graphs represents the mean fluorescence intensity of three independent experiments ± SE in MCF-7, DU-145, and CHO cells. *$P$ < 0.05 vs MCF-7 cells.

more attenuated in DU-145 cells ($IC_{50}$ = 6.80 ± 0.99) and CHO cells (5.8 ± 0,01) (Figure 7B) (Table 3).

In order to determine if the cytotoxic activity of **6** was related to the receptor expression on the cell surface, we next characterized the $sstr_2$ levels by flow cytometry. As shown in Figure 8A, $sstr_2$ expression was detected on the three cell lines. Notably, $sstr_2$ expression was significantly higher in the DU-145 and CHO cells than in MCF-7 cells (mean cell fluorescence intensity 347.5 ± 54.6, 344.0 ± 50.56, and 206.7 ± 14.27, respectively) (Figure 8B), which demonstrates that the cytotoxic activity of **6** is strongly correlated with $sstr_2$ expression levels, especially in the DU-145 and MCF7 cells. However, although the CHO cells displayed similar $sstr_2$ expression levels to DU-145, the toxicity of **6** was attenuated in these cells, suggesting some selective cytotoxic activity of the ruthenium−octreotide conjugate toward cancer cells with respect to normal cells.

As a very weak expression of $sstr_2$ has been previously reported in CHO cells,[69] the $sstr_2$ expression in this cell line was additionally examined according to their mRNA expression levels. PCR analyses confirmed $sstr_2$ gene expression in CHO cells, with similar mRNA levels than in MCF-7 cells (see the Supporting Information). Our results are in keeping with different studies describing that somatostatin receptors can also be identified in a broad panel of normal tissues, as well as in the human immune system.[70] As a consequence, new clinical applications for somatostatin analogues in several benign pathological diseases are emerging in addition to their role in malignant diseases.

All together, our results demonstrate a good correlation between the antitumor activity of the ruthenium−octreotide conjugate **6** and the expression of the $sst_2$ receptor on the cell surface and reveal the potential of conjugation with receptor-binding peptides such as octreotide to deliver metal-based anticancer drugs specifically to cells overexpressing somatostatin subtype-2 receptor.

## CONCLUSIONS

In summary, in this work we have described a straightforward solid-phase methodology for the conjugation of a dichloridoplatinum(II) complex as well as three "piano-stool" organometallic ruthenium(II) and osmium(II) complexes to a dicarba analogue of octreotide, a potent somatostatin agonist whose receptors, particularly subtype 2, are overexpressed on the membrane of tumor cells. At nuclear $Cl^-$ concentration (4 mM), platinum (**3**), osmium (**4**), and Ru(dap) (**5**) conjugates are activated through hydrolysis of the M-Cl, which correlates well with their DNA binding capacity, revealing in all cases a strong preference for guanine nucleobases. However, neither hydrolysis of the Ru−Cl nor interaction with DNA was observed in the case of the triphenylphosphine-containing ruthenium conjugate (**6**). Surprisingly, the latter conjugate displays antiproliferative activity, but the rest of the conjugates were noncytotoxic. Additional cytotoxic experiments with control metal complexes and cellular uptake experiments by ICP-MS, as well as conformational analysis of metal−octreotide conjugates by 2D NMR spectroscopy and molecular dynamics calculations, have allowed us to establish three general conclusions. First, a significant loss in the cytotoxic activity of the metal complex moiety always occurs when conjugated to the peptide sequence (e.g., $IC_{50}$ = 3.32 ± 0.54 in MCF-7 cells and $IC_{50}$ = 6.80 ± 0.99 in DU-145 cells for complex **17** vs $IC_{50}$ = 63.00 ± 1.53 in MCF-7 cells and $IC_{50}$ = 26.00 ± 2.00 in DU-145 cells for conjugate **6**); hence, it seems to be important to use metal complexes with high cytotoxic activity in order to develop peptide-conjugates with active biological properties. Second, despite the presence of some altered amino acids in the pharmacophore sequence of octreotide, particularly at the *N*-terminal end of the peptide, the overall structure is essentially maintained in the conjugate, which suggests that the affinity for somatostatin receptors would not be compromised upon conjugation to a metal complex; this observation is in good agreement with the higher accumulation of ruthenium in cancer cells upon exposure to the ruthenium−octreotide conjugate **6** in comparison with that of the parent complex **17**, which

demonstrates that the peptide has a positive effect on the internalization of the ruthenium complex. The choice of the spacer is also important, not only to improve aqueous solubility and to keep the metal complex away from the peptide, but also to reduce conformational freedom between both fragments in the conjugate. Third, the significantly higher expression of the $sst_2$ receptor on DU-145 cells compared to MCF-7 cells is in good agreement with $IC_{50}$ values of conjugate **6** in both tumor cell lines. The fact that control complex **17** shows an attenuated cytotoxicity in DU-145 cells compared with MCF-7 cells supports that the antitumoral activity of the ruthenium–octreotide conjugate **6** is correlated with the overexpression of the $sst_2$ receptor on the cell surface. The cytotoxic activity of **6** in a nontumor cell line (CHO) was similar to that found in cancer cells, a result which can be attributed to a similar level of expression of somatostatin subtype-2 receptors.

The overall results of this work demonstrate the potential of conjugation between metal-based anticancer drugs and receptor-binding peptides such as octreotide to target tumoral cells through binding to specific receptors, including somatostatin subtype 2 receptor, overexpressed in their membranes. In the near future, this receptor-targeted anticancer strategy is expected to generate new antitumor drugs with reduced side-effects and reduced toxicity in normal cells. The potential of this strategy will be increased by using novel approaches to circumvent some of the limitations found in this work, particularly new biological vectors in combination with photoactivated metal complexes[25] or cleavable linkers[32] in the biological media. Work is in progress in this direction to generate more specific metal-based anticancer drugs.

## ■ ASSOCIATED CONTENT

### Supporting Information

Selected MS spectra and HPLC traces of metal complex–octreotide conjugates and of DNA–conjugate adducts. NMR data of conjugates **3**, **4**, and **6**, and of control metal complexes. sstr2 mRNA expression in CHO and MCF-7 cells. This material is available free of charge via the Internet at http://pubs.acs.org.

## ■ AUTHOR INFORMATION

### Corresponding Author

*Vicente Marchán: Phone +34 934021249, Fax +34 933397878, E-mail vmarchan@ub.edu. Anna Massaguer: Phone +34 972418370, Fax +34 972418150, E-mail anna.massaguer@udg.edu.

### Author Contributions

[#]Both authors contributed equally to this work.

### Notes

The authors declare no competing financial interest.

## ■ ACKNOWLEDGMENTS

This work was supported by funding from the Ministerio de Educación y Ciencia (CTQ2005-01834, CTQ2007-68014, CTQ2008-02064, and CTQ2010-21567), the Generalitat de Catalunya (2009SGR208 and Xarxa de Referència de Biotecnologia), Instituto de Salud Carlos III (grants RD06/0020/0041), the Programa d'Intensificació de la Recerca (UB) and the ERC (grant no 247450, to PJS). We thank Prof. Alfonso Carotenuto (University of Napoli) for providing the coordinates of the dicarba analogue of octreotide **2**, Dr. Sabine H. van Rijt (University of Warwick) for supplying the osmium complex **8**, and Dr. Isolda Romero (University of Warwick) and Dr. Antoni Padró (Centres Científics i Tecnològics, Universitat de Barcelona) for helpful assistance in the determination of ruthenium content by ICP-MS.

## ■ ABBREVIATIONS USED

Abu, aminoisobutyryl; ACN, acetonitrile; bip, biphenyl; cym, cymene (1-methyl-4-(1-methylethyl)benzene); dap, 1-(carboxylic acid)-1,2-diaminoethane; DCM, dichloromethane; dhDsa*C*, dehydrodiaminosuberic acid *C*-terminus; dhDsa*N*, dehydrodiaminosuberic acid *N*-terminus; DIPC, *N,N′*-diisopropylcarbodiimide; DIPEA, *N,N*-diisopropylethylamine; DMF, *N,N*-dimethylformamide; DMSO, dimethylsulfoxide; DTPA, diethylenetriamino-pentaacetic acid; DOTA, 1,4,7,10-tetraazacyclododecane-1,4,7,10-tetraacetic acid; Dsa*C*, diaminosuberic acid *C*-terminus; Dsa*N*, diaminosuberic acid *N*-terminus; ESI, electrospray ionization; Fluo, 5(6)-carboxyfluorescein; Fmoc, 9-fluorenylmethyloxycarbonyl; Hag, L-2-allylglycine; HATU, hexafluorophosphate salt of the (2-(7-aza-1*H*-benzotriazol-1-yl)-1,1,3,3-tetramethyluronium; HOAt, 1-hydroxy-7-azabenzotriazole; HOBt, 1-hydroxybenzotriazole; HR-ESI, high-resolution electrospray ionization; ICP-MS, inductively coupled plasma mass spectrometry; Im, imidazole; Ind, indazole; MALDI-TOF, matrix-assisted laser desorption ionization time-of-flight; MS, mass spectrometry or mass spectrum; MTT, 3-(4,5-dimethylthiazol-2-yl)-2,5-diphenyltetrazolium bromide; NHS, *N*-hydroxysuccinimide; NOE, nuclear Overhauser effect; NOESY, nuclear Overhauser enhanced spectroscopy; PBS, phosphate buffered saline; PEG, poly(ethylene glycol); pico, picolinate; sst, somatostatin; sstr, somatostatin receptor; TIS, triisopropylsilane; TMP, trimethylphosphite; TFA, trifluoroacetic acid

## ■ REFERENCES

(1) Reubi, J. C. (2003) Peptide receptors as molecular targets for cancer diagnosis and therapy. *Endocr. Rev. 24*, 389–427.

(2) Zaccaro, L., del Gatto, A., Pedone, C., and Saviano, M. (2009) Peptides for tumour therapy and diagnosis: Current status and future directions. *Curr. Med. Chem. 16*, 780–795.

(3) Okarvi, S. M. (2008) A comprehensive overview of peptide-based radiopharmaceuticals and cytotoxic conjugates, as well as their potential applications in cancer diagnosis and therapy. *Cancer Treat. Rev. 34*, 13–26.

(4) Mezo, G., and Manea, M. (2010) Receptor-mediated tumor targeting based on peptide hormones. *Expert Opin. Drug Delivery 7*, 79–96.

(5) Schaer, J. C., Waser, B., Mengod, G., and Reubi, J. C. (1997) Somatostatin receptor subtype expression in human pituitary, gastroentero-pancreatic and mammary tumors: comparison of mRNA analysis with receptor autoradiography. *Int. J. Cancer 70*, 530–537.

(6) Janecka, A., Zubrzycka, M., and Janecki, T. (2001) Somatostatin analogs. *J. Pept. Res. 58*, 91–107.

(7) Bauer, W., Briner, U., Dopfener, W., Haller, R., Huguenin, R., Marbach, P., Petcher, T. J., and Pless, J. (1982) SMS 201–995: a very potent and selective analogue of somatostatin with prolonged action. *Life Sci. 31*, 1133–1140.

(8) de Jong, M., Breeman, W. A. P., Kwekkeboom, D. J., Valkema, R., and Krenning, E. P. (2009) Tumor imaging and therapy using radiolabeled somatostatin analogues. *Acc. Chem. Res. 42*, 873–880.

(9) Sun, L.-C., and Coy, D. H. (2008) Cytotoxic conjugates of peptide hormones for cancer chemotherapy. *Drugs Future 33*, 217–223.

(10) Wheate, N. J., Walker, S., Craig, G. E., and Oun, R. (2010) The status of platinum anticancer drugs in the clinic and in clinical trials. *Dalton Trans. 39*, 8113−8127.
(11) Jakupec, M. A., Galanski, M., Arion, V. B., Hartinger, C. G., and Keppler, B. K. (2008) Antitumour metal compounds: more than theme and variations. *Dalton Trans.*, 183−194.
(12) van Rijt, S. H., and Sadler, P. J. (2009) Current applications and future potential for bioinorganic chemistry in the development of anticancer drugs. *Drug Discovery Today 14*, 1089−1097.
(13) Rademaker-Lakhai, J. M., Van den Bongard, D., Pluim, D., Beijnen, J. H., and Schellens, J. H. M. (2004) A phase I and pharmacological study with imidazolium-*trans*-DMSO-imidazole-tetrachlororuthenate, a novel ruthenium anticancer agent. *Clin. Cancer Res. 10*, 3717−3727.
(14) Jakupec, M. A., Arion, V. B., Kapitza, S., Reisner, E., Eichinger, A., Pongratz, M., Marian, B., Graf von Keyserlingk, N., and Keppler, B. K. (2005) KP1019 (FFC14A) from bench to bedside: preclinical and early clinical development - an overview. *Int. J. Clin. Pharmacol. Ther. 43*, 595−596.
(15) Peacock, A. F. A., and Sadler, P. J. (2008) Medicinal organometallic chemistry: Designing metal arene complexes as anticancer agents. *Chem. Asian J. 3*, 1890−1899.
(16) Levina, A., Mitra, A., and Lay, P. A. (2009) Recent developments in ruthenium anticancer drugs. *Metallomics 1*, 458−470.
(17) Casini, A., Hartinger, C. G., Nazarov, A., and Dyson, P. J. (2010) Organometallic antitumour agents with alternative modes of action. *Top. Organomet. Chem. 32*, 57−80.
(18) Gasser, G., Ott, I., and Metzler-Nolte, N. (2011) Organometallic anticancer compounds. *J. Med. Chem. 54*, 3−25.
(19) Süss-Fink, G. (2010) Arene ruthenium complexes as anticancer agents. *Dalton Trans. 39*, 1673−1688.
(20) Wang, F., Chen, H., Parsons, S., Oswald, I. D. H., Davidson, J. E., and Sadler, P. J. (2003) Kinetics of aquation and anation of ruthenium(II) arene anticancer complexes, acidity and X-ray structures of aqua adducts. *Chem.—Eur. J. 9*, 5810−5820.
(21) Kostrhunova, H., Florian, J., Novakova, O., Peacock, A. F. A., Sadler, P. J., and Brabec, V. (2008) DNA interactions of monofunctional organometallic osmium(II) antitumor complexes in cell-free media. *J. Med. Chem. 51*, 3635−3643.
(22) Pizarro, A. M., Habtemariam, A., and Sadler, P. J. (2010) Activation mechanisms for organometallic anticancer complexes. *Top. Organomet. Chem. 32*, 21−56.
(23) Barragán, F., Moreno, V., and Marchán, V. (2009) Solid-phase synthesis and DNA binding studies of dichloroplatinum(II) conjugates of dicarba analogues of octreotide as new anticancer drugs. *Chem. Commun.*, 4705−4707.
(24) D'Addona, D., Carotenuto, A., Novellino, E., Piccand, V., Reubi, J. C., Di Cianni, A., Gori, F., Papini, A. M., and Ginanneschi, M. (2008) Novel sst5-selective somatostatin dicarba-analogs: Synthesis and conformation-affinity relationships. *J. Med. Chem. 51*, 512−520.
(25) Barragán, F., López-Senín, P., Salassa, S., Betanzos-Lara, S., Habtemariam, A., Moreno, V., Sadler, P. J., and Marchán, V. (2011) Photocontrolled DNA binding of a receptor-targeted organometallic ruthenium(II) complex. *J. Am. Chem. Soc. 133*, 14098−14108.
(26) Dirscherl, G., and König, B. (2008) The use of solid-phase synthesis techniques for the preparation of peptide-metal complex conjugates. *Eur. J. Org. Chem.*, 597−634.
(27) Metzler-Nolte, N. (2010) Biomedical applications of organometal-peptide conjugates. *Top. Organomet. Chem. 32*, 195−217.
(28) Peindy N'Dongo, H. W., Ott, I., Gust, R., and Schatzschneider, U. (2009) Microwave-assisted solid-phase synthesis, cellular uptake, and cytotoxicity studies of cymantrene-peptide bioconjugates. *J. Organomet. Chem. 694*, 823−827.
(29) Gross, A., and Metzler-Nolte, N. (2009) Synthesis and characterization of a ruthenocenoyl bioconjugate with the cyclic octapeptide octreotate. *J. Organomet. Chem. 694*, 1185−1188.
(30) van Rijt, S. H., Kostrhunova, H., Brabec, V., and Sadler, P. J. (2011) Functionalization of osmium arene anticancer complexes with (Poly)arginine: effect on cellular uptake, internalization, and cytotoxicity. *Bioconjugate Chem. 22*, 218−226.
(31) Puckett, C. A., and Barton, J. K. (2010) Targeting a ruthenium complex to the nucleus with short peptides. *Bioorg. Med. Chem. 18*, 3564−3659.
(32) Splith, K., Hu, W., Schatzschneider, U., Gust, R., Ott, I., Onambele, L. A., Prokop, A., and Neundorf, I. (2010) Protease-activatable organometal-peptide bioconjugates with enhanced cytotoxicity on cancer cells. *Bioconjugate Chem. 21*, 1288−1296.
(33) Mukhopadhyay, S., Barnes, C. M., Haskel, A., Short, S. M., Barnes, K. R., and Lippard, S. J. (2008) Conjugated platinum(IV)-peptide complexes for targeting angiogenic tumor vasculature. *Bioconjugate Chem. 19*, 39−49.
(34) Hsieh, H.-P., Wu, Y.-T., Chen, S.-T., and Wang, K.-T. (1999) Direct solid-phase synthesis of octreotide conjugates: precursors for use as tumor-targeted radiopharmaceuticals. *Bioorg. Med. Chem. 7*, 1797−1803.
(35) Moradell, S., Lorenzo, J., Rovira, A., Robillard, M. S., Aviles, F. X., Moreno, V., de Llorens, R., Martinez, M. A., Reedijk, J., and Llobet, A. (2003) Platinum complexes of diaminocarboxylic acids and their ethyl ester derivatives: the effect of the chelate ring size on antitumor activity and interactions with GMP and DNA. *J. Inorg. Biochem. 96*, 493−502.
(36) van Rijt, S. H., Peacock, A. F. A., Johnstone, R. D. L., Parsons, S., and Sadler, P. J. (2009) Organometallic osmium(II) arene anticancer complexes containing picolinate derivatives. *Inorg. Chem. 48*, 1753−1762.
(37) Hodson, E., and Simpson, S. J. (2004) Synthesis and characterization of $[(\eta 6\text{-cymene})\mathrm{Ru(L)X_2}]$ compounds: single crystal X-ray structure of $[(\eta 6\text{-cymene})\mathrm{Ru(P\{OPh\}_3)Cl_2}]$ at 203 K. *Polyhedron 23*, 2695−2707.
(38) Chaplin, A. B., and Dyson, P. J. (2007) Catalytic activity of bis-phosphine ruthenium(II)-arene compounds: Structure-activity correlations. *Organometallics 26*, 2447−2455.
(39) Charvat, T. T., Lee, D. J., Robinson, W. E., and Chamberlin, A. R. (2006) Design, synthesis, and biological evaluation of chicoric acid analogs as inhibitors of HIV-1 integrase. *Bioorg. Med. Chem. 14*, 4552−4567.
(40) Gariepy, J., Remy, S., Zhang, X., Ballinger, J. R., Bolewska-Pedyczak, E., Rauth, M., and Bisland, K. (2002) A simple two-step approach for introducing a protected diaminedithiol chelator during solid-phase assembly of peptides. *Bioconjugate Chem. 13*, 679−684.
(41) Marchán, V., Moreno, V., Pedroso, E., and Grandas, A. (2001) Towards a better understanding of the cisplatin mode of action. *Chem.—Eur. J. 7*, 808−815.
(42) Marchán, V., Pedroso, E., and Grandas, A. (2004) Insights into the reaction of transplatin with DNA and proteins: Methionine-mediated formation of histidine-guanine trans-$\mathrm{Pt(NH_3)_2}$ cross-links. *Chem.—Eur. J. 10*, 5369−5375.
(43) Algueró, B., López de la Osa, J., González, C., Pedroso, E., Marchán, V., and Grandas, A. (2006) Selective platination of modified oligonucleotides and duplex cross-links. *Angew. Chem., Int. Ed. 45*, 8194−8197.
(44) Goddard, D. T., and Kneller, G. *SPARKY*, University of California, San Francisco.
(45) Singh, S. K., Trivedi, M., Chandra, M., Sahay, A. N., and Pandey, D. S. (2004) Luminescent piano-stool complexes incorporating 1-(4-cyanophenyl)imidazole: Synthesis, spectral, and sructural studies. *Inorg. Chem. 43*, 8600−8608.
(46) Koradi, R., Billeter, M., and Wuthrich, K. (1996) MOLMOL: a program for display and analysis of macromolecular structures. *J. Mol. Graphics 14*, 29−32.
(47) Peacock, A. F. A., Parsons, S., and Sadler, P. J. (2007) Tuning the hydrolytic aqueous chemistry of osmium arene complexes with *N,O*-chelating ligands to achieve cancer cell cytotoxicity. *J. Am. Chem. Soc. 129*, 3348−3357.
(48) van Rijt, S. H., Mukherjee, A., Pizarro, A. M., and Sadler, P. J. (2010) Cytotoxicity, hydrophobicity, uptake, and distribution of

osmium(II) anticancer complexes in ovarian cancer cells. *J. Med. Chem. 53*, 840−849.
(49) Morris, R. E., Aird, R. E., Murdoch, P., del, S., Chen, H., Cummings, J., Hughes, N. D., Parsons, S., Parkin, A., Boyd, G., Jodrell, D. I., and Sadler, P. J. (2001) Inhibition of cancer cell growth by ruthenium(II) arene complexes. *J. Med. Chem. 44*, 3616−3621.
(50) Moreno, V., Font-Bardia, M., Calvet, T., Lorenzo, J., Aviles, F. X., Garcia, M. H., Morais, T. S., Valente, A., and Robalo, M. P. (2011) DNA interaction and cytotoxicity studies of new ruthenium(II) cyclopentadienyl derivative complexes containing heteroaromatic ligands. *J. Inorg. Biochem. 105*, 241−249.
(51) Gianferrara, T., Bratsos, I., and Alessio, E. (2009) A categorization of metal anticancer compounds based on their mode of action. *Dalton Trans. 37*, 7588−7598.
(52) Jennerwein, M., and Andrews, P. A. (1995) Effect of intracellular chloride on the cellular pharmacodynamics of cis-diamminedichloroplatinum(II). *Drug Metab. Dispos. 23*, 178−184.
(53) Wang, F., Habtemariam, A., van der Geer, E. P. L., Fernandez, R., Melchart, M., Deeth, R. J., Aird, R., Guichard, S., Fabbiani, F. P. A., Lozano-Casal, P., Oswald, I. D. H., Jodrell, D. I., Parsons, S., and Sadler, P. J. (2005) Controlling ligand substitution reactions of organometallic complexes: Tuning cancer cell cytotoxicity. *Proc. Natl. Acad. Sci. U.S.A. 102*, 18269−18274.
(54) Peacock, A. F. A., Habtemariam, A., Moggach, S. A., Prescimone, A., Parsons, S., and Sadler, P. J. (2007) Chloro half-sandwich osmium(II) complexes: influence of chelated *N,N*-ligands on hydrolysis, guanine binding, and cytotoxicity. *Inorg. Chem. 46*, 4049−4059.
(55) Novakova, O., Chen, H., Vrana, O., Rodger, A., Sadler, P. J., and Brabec, V. (2003) DNA Interactions of monofunctional organometallic ruthenium(II) antitumor complexes in cell-free media. *Biochemistry 42*, 11544−11554.
(56) Liu, H.-K., Wang, F., Parkinson, J. A., Bella, J., and Sadler, P. J. (2006) Ruthenation of duplex and single-stranded d(CGGCCG) by organometallic anticancer complexes. *Chem.—Eur. J. 12*, 6151−6165.
(57) Gossens, C., Tavernelli, I., and Rothlisberger, U. (2009) Binding of organometallic ruthenium(II) anticancer compounds to nucleobases: A computational study. *J. Phys. Chem. A 113*, 11888−11897.
(58) Kostrhunova, H., Florian, J., Novakova, O., Peacock, A. F. A., Sadler, P. J., and Brabec, V. (2008) DNA Interactions of monofunctional organometallic osmium(II) antitumor complexes in cell-free media. *J. Med. Chem. 51*, 3635−3643.
(59) Fischer, R., Mader, O., Jung, G., and Brock, R. (2003) Extending the applicability of carboxyfluorescein in solid-phase synthesis. *Bioconjugate Chem. 14*, 653−660.
(60) Watson, J. C., Balster, D. A., Gebhardt, B. M., O'Dorisio, T. M., O'Dorisio, M. S., Espenan, G. D., Drouant, G. J., and Woltering, E. A. (2001) Growing vascular endothelial cells express somatostatin subtype 2 receptors. *Br. J. Cancer 85*, 266−272.
(61) Hornick, C. A., Anthony, C. T., Hughey, S., Gebhardt, B. M., Espenan, G. D., and Woltering, E. A. (2000) Progressive nuclear translocation of somatostatin analogs. *J. Nucl. Med. 41*, 1256−1263.
(62) Zhang, Y., Wang, X., Wang, J., Zhang, X., and Zhang, Q. (2011) Octreotide-modified polymeric micelles as potential carriers for targeted docetaxel delivery to somatostatin receptor overexpressing tumor cells. *Pharm. Res. 28*, 1167−1178.
(63) Huang, C. M., Wu, Y. T., and Chen, S. T. (2000) Targeting delivery of paclitaxel into tumor cells via somatostatin receptor endocytosis. *Chem. Biol. 7*, 453−461.
(64) Wynants, C., Van Binst, G., and Loosli, H. R. (1985) SMS 201−995, a very potent analogue of somatostatin. Assignment of the 1H 500 MHz n.m.r. spectra and conformational analysis in aqueous solution. *Int. J. Pept. Protein Res. 25*, 608−614.
(65) Wynants, C., Van Binst, G., and Loosli, H. R. (1985) SMS 201−995, an octapeptide somatostatin analogue. Assignment of the 1H 500 MHz n.m.r. spectra and conformational analysis of SMS 201−995 in dimethylsulfoxide. *Int. J. Pept. Protein Res. 25*, 615−621.
(66) Melacini, G., Zhu, Q., and Goodman, M. (1997) Multiconformational NMR Analysis of sandostatin (octreotide): equilibrium between $\beta$-sheet and helical structures. *Biochemistry 36*, 1233−1241.
(67) Deshmukh, M. V., Voll, G., Kuehlewein, A., Maecke, H., Schmitt, J., Kessler, H., and Gemmecker, G. (2005) NMR studies reveal structural differences between the Gallium and Ytrium complexes of DOTA-D-Phe1-Tyr3-octreotide. *J. Med. Chem. 48*, 1506−1514.
(68) Reubi, J. C., Schar, J. C., Waser, B., Wenger, S., Heppeter, A., Schmitt, J. S., and Mäcke, H. R. (2000) Affinity profiles for human somatostatin receptor subtypes sstr1-sstr5 of somatostatin radiotracers selected for scintigraphic and radiotherapeutic use. *Eur. J. Nucl. Med. 27*, 273−282.
(69) Zhang, J., Jin, W., Wang, X., Wang, J., Zhang, X., and Zhang, Q. (2010) A novel octreotide modified lipid vesicle improved the anticancer efficacy of doxorubicin in somatostatin receptor 2 positive tumor models. *Mol. Pharm. 7*, 1159−1168.
(70) Cascini, G. L., Cuccurullo, V., and Mansi, L. (2010) The non tumour uptake of (111)In-octreotide creates new clinical indications in benign diseases, but also in oncology. *Q. J. Nucl. Med. Mol. Imaging 54*, 24−36.